An investigation into atmospheric nitrous acid (HONO) processes in South Korea

Kiyeon Kim[1], Kyung M. Han[1*], Chul H. Song[1*], Hyojun Lee[1], Ross Beardsley[2], Jinhyeok Yu[1], Greg Yarwood[2], Bonyoung Koo[3], Jasper Madalipay[1], Jung-Hun Woo[4], and Seogju Cho[5]

1. School of Earth Sciences and Environmental Engineering, Gwangju Institute of Science and Technology (GIST), Gwangju 61005, Republic of Korea
2. Ramboll USA, Novato, CA 94945, USA
3. Bay Area Air Quality Management District, San Francisco, CA 94105, USA
4. Department of Technology Fusion Engineering, College of Engineering, Konkuk University, Seoul 05029, Republic of Korea
5. Seoul Metropolitan Government Research Institute of Public Health Environment, 30, Janggunmaeul 3-gil, Gwacheon-si, Gyeonggi-do 13818, Republic of Korea

Short title: Atmospheric HONO processes

* **Corresponding authors:** Kyung Man Han (kmhan@gist.ac.kr) and Chul Han Song (chsong@gist.ac.kr)

(Submitted to ***Atmospheric Chemistry and Physics***)

Abstract

Nitrous acid (HONO) is a main precursor of hydroxyl radicals (OH), which contribute to the formation of numerous secondary air pollutants in the troposphere. Despite its importance in atmospheric chemistry, HONO chemistry has not been fully incorporated into many chemical transport models (CTMs). Due to the lack of atmospheric HONO processes, CTM simulations often tend to underestimate atmospheric mixing ratios of HONO. This study was undertaken because simulations with current Community Multiscale Air Quality (CMAQ) model have a strong tendency to underestimate the HONO mixing ratio. In search of missing sources of atmospheric HONO, we attempted to sequentially incorporate the following potential HONO sources and processes into the CMAQ modeling framework: (i) gas-phase HONO reactions; (ii) traffic HONO emissions; (iii) soil HONO emissions; (iv) heterogeneous HONO production on the surfaces of aerosols; (v) heterogeneous HONO formation on tree leaf and building surfaces; (vi) photolysis reactions of particulates and deposited HNO_3/nitrates called 'renoxification'. The simulation performances of the modified CMAQ models were then evaluated by comparing the modeled HONO mixing ratios with the HONO mixing ratios observed at the Olympic Park station in Seoul, South Korea. When HONO processes were fully added to the CMAQ model, average daily HONO mixing ratios increased from 0.06 ppb to 1.18 ppb. The daytime HONO mixing ratios produced from the CMAQ model run with a full account of atmospheric HONO processes were found to be in better agreement with observations than those from the original CMAQ model (CMAQv5.2.1) runs with improved statistical metrics (e.g., IOA increased from 0.59 to 0.68, while MB decreased dramatically from -0.57 ppb to -0.34 ppb). In addition, we investigated the contributions of individual atmospheric HONO processes to HONO mixing ratios, as well as the impacts of HONO atmospheric processes on the concentrations of other atmospheric species in South Korea. All these issues are also discussed in this manuscript.

Keywords: Nitrous acid (HONO); Heterogeneous HONO production; CMAQ model; Ozone production rate.

1. Introduction

Hydroxyl radicals (OH) play a key role in atmospheric chemistry. OH radicals oxidize volatile organic compounds (VOCs), sulfur dioxide (SO_2), and nitrogen dioxide (NO_2), contributing to the formation of secondary organic and inorganic aerosols (Pathak et al., 2009). Therefore, accurate determination of the mixing ratio of OH radicals is crucial to understanding atmospheric photochemistry in both polluted and remote areas.

Nitrous acid (HNO_2 or HONO) has been recognized as a main precursor of OH radicals via photo-dissociation (R1) (Harris et al., 1982; Alicke et al., 2003; Kleffmann et al., 2005):

$$\mathrm{HONO} + h\nu \xrightarrow{j_{HONO}} \mathrm{OH} + \mathrm{NO}\ (300\ \mathrm{nm} < \lambda < 405\ \mathrm{nm}) \qquad \text{(R1)}$$

Several studies have estimated that HONO photolysis reactions contribute 20 – 80% of OH radicals and 30 – 87% of HO_x formation in polluted urban areas (Alicke et al., 2003; Ren et al., 2003; Kleffmann et al., 2005; Acker et al., 2006; Monks et al., 2009; Hendrick et al., 2014; Kim et al., 2014). However, it was also recognized that the HONO chemistry was not yet fully understood.

Therefore, many field measurements have been carried out to characterize atmospheric HONO processes (Su et al., 2008; Li et al., 2012; Kim et al., 2014; Lee et al., 2016). These studies showed that the observed HONO mixing ratios were significantly higher than those predicted by atmospheric chemistry-transport model simulations (Su et al., 2008; Vandenboer et al., 2013; Li et al., 2014; Lee et al., 2016). This indicates that there should be missing HONO sources or processes that are not considered in current atmospheric models (CTMs).

Recent studies have proposed incorporating several HONO production pathways into chemical transport models to explain the missing HONO processes. Suggested sources include i) traffic HONO emissions (Kirchstetter et al., 1996; Kurtenbach et al., 2001; Rappenglück et al., 2013; Czader et al., 2015; Xu et al., 2015; Nakashima and Kajii, 2017; Li et al., 2018); ii)

soil HONO emissions (Nagai and Kubota, 1972; Oswald et al., 2013; Weber et al., 2015; Meusel et al., 2016); iii) HONO emissions from biomass burning (Crutzen and Andreae, 1990; Cheng et al., 2014; Nie et al., 2015); iv) indoor HONO emissions (Gligorovski, 2016; Zhang et al., 2019); and iv) heterogeneous conversion of NO_2 to HONO on the surfaces of aerosols, grounds, and leaves (Svensson et al., 1987; Wiesen et al., 1995; Reisinger, 2000; Han et al., 2017).

Among these processes, traffic HONO emissions were reported to be the key factor influencing the HONO mixing ratio in the Beijing–Tianjin–Hebei (BTH) region at night (Zhang et al., 2019). Heterogeneous NO_2 reactions on aerosol surfaces were an important source of HONO during the severe haze period in Beijing (Jia et al., 2020). On the other hand, Zhang et al. (2016) reported that heterogeneous reactions on ground surfaces could be the dominant source of atmospheric HONO, accounting for ~42% of the HONO mixing ratios in Hong Kong suburban areas.

These findings may indicate that atmospheric HONO production and a potential cause of discrepancies between modeled and observed HONO mixing ratios may vary temporally and regionally. In addition, no research has been conducted on which sources of HONO control the levels of HONO in Seoul, South Korea. In this context, the aims of this study are three-fold: i) to determine which HONO sources or processes are significant in South Korea; ii) to estimate the budget of the HONO mixing ratios from various HONO sources; and iii) achieving objectives i) and ii) to develop a near-perfect CTM in terms of HONO mixing ratio. To accomplish these goals, we decided to improve the US EPA CMAQ v5.2.1 model by incorporating several HONO production pathways including i) homogeneous HONO reactions; ii) direct HONO emissions from biomass burning, traffic vehicles, and soil; iii) heterogeneous HONO production on the surfaces of atmospheric aerosols, buildings, and tree leaves; and iv) photolysis reactions of particulate and deposited HNO_3/nitrate (renoxification).

We then tested the performances of the modified CMAQ models by comparing the modeled HONO mixing ratios with the HONO mixing ratios observed during the Korea-United States Air Quality (KORUS-AQ) campaign. After the comparison analysis, we evaluated the contributions of individual HONO processes to the HONO budget in South Korea and also investigated the effects of the HONO mixing ratios on the levels of other important atmospheric species.

2. Methodology

In this study, we incorporated various HONO sources and reactions into the CMAQ model framework to accurately estimate HONO mixing ratios in the atmosphere. Then, the simulation results of the modified CMAQ models were analyzed, comparing the modeled outputs with observations during the KORUS-AQ campaign. Details of the modifications of CMAQ models, the HONO measurements, and potentially important HONO sources considered in this study are described in the following sections.

2.1. WRF-CMAQ model configuration

Simulation of the Community Multiscale Air Quality (CMAQ) v5.2.1 model (Byun and Schere, 2006) was carried out to estimate the HONO mixing ratios during the period of the KORUS-AQ campaign (9 May – 12 June, 2016). Figure 1 shows the horizontal domain (A1) for the CMAQ model simulation. The spatial domain has 273×204 grid cells with a horizontal resolution of 15 × 15 km^2 and contains 15 vertical layers with the first layer at ~34 m above the ground.

The photochemical mechanism used in the simulation of the CMAQ model was the Statewide Air Pollution Research Center-07 (SAPRC-07 TC) (Carter, 2010; Hutzell et al., 2012). The AERO6 module was used for aerosol calculations (Binkowski and Roselle, 2003). In particular, the heterogeneous reactions considered in this study were embedded into the

SAPRC-07 TC via the Korean Flexible Chemistry (KFC) editor. The KFC editor is a chemical mechanism editor in a framework of Graphic User Interface (GUI) developed to quickly implement the modifications of the chemical mechanisms of the CMAQ model. The details of the heterogeneous reactions we considered are discussed in Sects. 2.3.5 – 2.3.6.

The Weather Research and Forecasting (WRF) v3.8.1 model (Skamarock et al., 2008) was run to generate meteorological fields that drive the CMAQ model. The physical options used in the WRF run are as follows: i) WRF Single-Moment 6-class Microphysics scheme (Hong and Lim, 2006); ii) Rapid radiative transfer model (RRTMG) for longwave and shortwave radiation (Iacono et al., 2008); iii) the NOAH Land Surface scheme (Chen and Dudhia, 2001); iv) Yonsei University (YSU) Planetary Boundary Layer (PBL) scheme (Hong et al., 2006); v) MM5 surface layer scheme (Jiménez et al., 2012); and vi) the Grell-Freitas Ensemble scheme for cumulus physics (Grell and Freitas, 2014). Initial and boundary conditions for the WRF model runs were obtained from the National Center for Environmental Prediction Final Analysis (NCEP-FNL) every six hours.

For anthropogenic emissions, this study used the KORUS v5.0 inventory processed by the Sparse Matrix Operator Kernel Emissions in Asia (SMOKE-Asia; Woo et al., 2012) (Woo et al., 2020). The KORUS v5.0 emissions were developed particularly for CTM runs as part of the KORUS-AQ campaign. Biogenic emissions were generated using the Model of Emissions of Gases and Aerosol from Nature (MEGAN) v2.10 (Guenther et al., 2012). Fire emissions were obtained from the Fire Inventory from NCAR (FINN) v1.5 emission inventory (https://bai.acom.ucar.edu/Data/fire/; Wiedinmyer et al., 2011). The various HONO emissions considered in this study are discussed in Sects. 2.3.2. – 2.3.4.

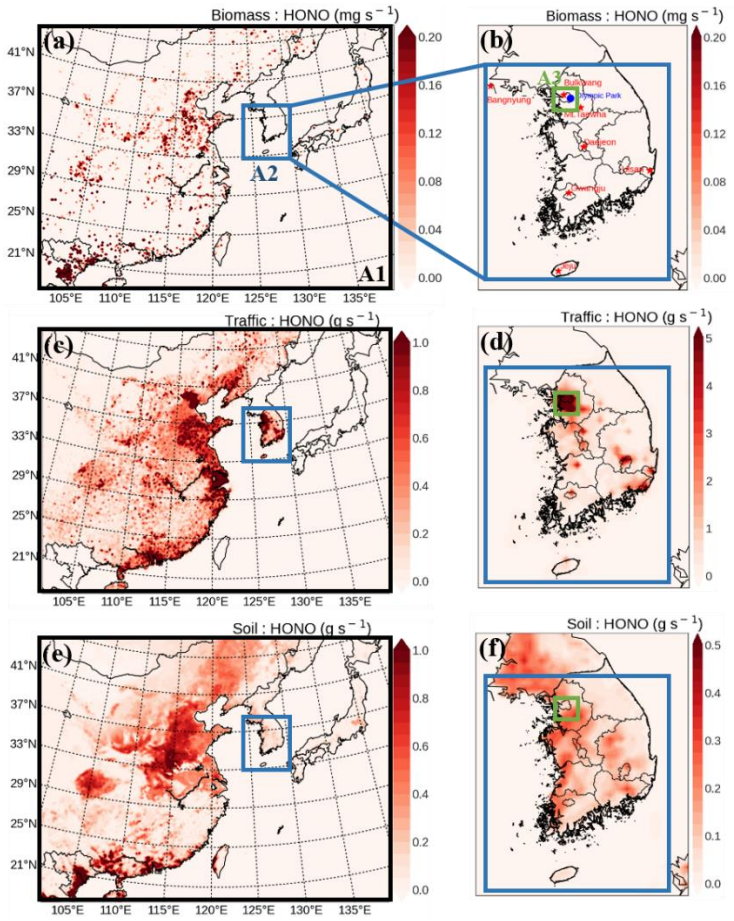

146

147 **Figure 1. S**patial distributions of HONO emission rates from biomass burning (panels (a) and
148 (b)), from traffic (panels (c) and (d)), and from soil (panels (e) and (f)) over East Asia (A1),
149 South Korea (A2), and the Seoul Metropolitan Area (A3). Several super-monitoring stations
150 are located at Bangnyung-Do, Bulkwang-Dong, Olympic Park, Mt.Taehwa, Daejeon, Gwangju,
151 Ulsan, and Jeju. The locations of these super-stations are shown in panel (b).

152 **2.2 Measurements**

153 During the KORUS-AQ campaign period, concentrations of NO_2, O_3, and particulate
154 matter were measured at several locations such as Olympic Park (37.52N; 127.12E),
155 Bangnyung (37.96N; 124.64E), Bulkwang (37.61N; 126.93E), Mt. Taewha (37.31N; 127.31E),
156 Daejeon (36.35N; 127.38E), Gwangju (35.23N; 126.84E), Ulsan (35.53N; 129.31E), and Jeju
157 (33.32N; 126.40E) (refer to Fig. 1b regarding the locations). In this study, we also used data
158 observed at approximately 320 stations from the AIR-KOREA network
159 (https://www.air.korea.or.kr), officially managed by the Korean Ministry of Environment in
160 South Korea.

Surface data observed at the Olympic Park station in Seoul were used for direct comparisons between simulated and observed HONO mixing ratios. These HONO mixing ratios were measured using the Monitor for AeRosols and GAses in ambient air (MARGA ADI 2080) (Applikon-ECN, Netherlands) instrument with a time resolution of 1 hour. This measurement is based on the wet-denuder-ion-chromatography (WD/IC) method. In the WD/IC system, HONO molecules absorbed by the solution in the denuder were converted to nitrite (NO_2^-), and then the nitrite concentrations were quantified by ion chromatography (Xu et al., 2019). The detection limit of the MARGA instrument for HONO is ~0.02 ppb. At the Olympic Park station, NO_2 and O_3 were also measured using commercially available instruments, EC9841 and EC9810, respectively, manufactured by Ecotech. Their detection limits for both species are ~0.5 ppb during the daytime. Details on the principles of EC9841 and EC9810 can be found in Keywood et al. (2019). $PM_{2.5}$ at the Olympic Park station were measured continuously using a Thermo Scientific Continuous Particulate Monitor, FH62C14, based on the beta attenuation method. The detection limit of the instrument is $4 \mu g/m^3$ in hourly measurements. Further information about instruments is provided in Table S1.

Meteorological data on temperature, relative humidity, pressure, wind speeds, and wind directions were also measured by the Automated Synoptic Observing System (ASOS) at the Olympic Park station. In order to test the simulation performances of the WRF-CMAQ model, observed meteorological data was compared with the modeled outputs, which is shown in Figure S1 and Table S2. In general, WRF model simulations tended to accurately predict meteorological fields.

Table 1. Comparison of parameterizations of HONO processes between CMAQ v5.2.1 and this study.

	HONO processes	CMAQ v5.2.1	This study	Ref.
Reaction	(R1) $HONO + hv \xrightarrow{j_{HONO}} OH + NO$	J_{HONO}	J_{HONO}	1
	(R2) $NPHE + hv \xrightarrow{j_{NPHE}} HONO + xPROD2$	$J_{NPHE} = 1.50e^{-3} \times J_{NO_2}$	$J_{NPHE} = 1.50e^{-3} \times J_{NO_2}$	
	(R3) $OH + NO + M \xrightarrow{k_3} HONO$	$k_3 = \{\frac{k_a[M]}{(1+k_a[M]/k_b)}\}0.6^{\frac{1}{1+[\log_{10}(\frac{k_a[M]}{k_b})]^2}}$ ▪ $k_a = 7.0\times 10^{-31}(\frac{T}{300})^{-2.6}$, ▪ $k_b = 3.6\times 10^{-11}(\frac{T}{300})^{-0.1}$	▪ $k_a = 7.1\times 10^{-31}(\frac{T}{300})^{-2.6}$, ▪ $k_b = 3.6\times 10^{-11}(\frac{T}{300})^{-0.1}$	2
	(R4) $HONO + OH \xrightarrow{k_4} H_2O + NO_2$	$k_4 = 2.5\times 10^{-12}e^{(\frac{-260}{T})}$	$k_4 = 3.0\times 10^{-12}e^{(\frac{-250}{T})}$	
	(R5) $2NO_2 + H_2O \xrightarrow{k_{aerosol}} HONO + HNO_3$	$k_{aerosol} = 1.0\times 10^{-4}(S/V)$	$k_{aerosol} = \frac{1}{4}v_{NO2}(S/V) \times \gamma_{a\_NO_2}$ Daytime: $\gamma_{a\_NO_2} = 1.3\times 10^{-4} \times \frac{\text{light intensity}}{900(W\cdot M^{-2})}$ Nighttime: $\gamma_{a\_NO_2} = 8.0\times 10^{-6}$	3, 4 5
	(R6) $2NO_2 + H_2O \xrightarrow{k_{ground}} HONO + HNO_3$	$k_{ground} = 5.0\times 10^{-5} \times (\frac{S_{g,building}}{V} + \frac{S_{g,leaf}}{V})$ ▪ $\frac{S_{g,leaf}}{V} = \frac{2\times LAI}{H}$ ▪ $\frac{S_{g,building}}{V} = PURB \times \frac{0.2\frac{m^2}{m^3}}{100\%}$	$k_{ground} = \frac{1}{8} \times V_{NO_2} \times \gamma_{g\_NO_2} \times (\frac{S_{g,building}}{V} + \frac{S_{g,leaf}}{V})$ ▪ $\frac{S_{g,leaf}}{V} = \frac{2\times LAI}{H}$ ▪ $\frac{S_{g,building}}{V} = PURB \times \frac{0.3\frac{m^2}{m^3}}{100\%}$ Daytime: $\gamma_{g\_NO_2} = 5.8\times 10^{-6} \times \frac{\text{light intensity}}{900(W\cdot M^{-2})}$ Nighttime: $\gamma_{g\_NO_2} = 5.0\times 10^{-7}$	6 7 4, 8 9
	(R7) $pNO_3 + hv \xrightarrow{J_{pNO_3}} 0.67HONO + 0.33NO_2$	-	$J_{pNO_3} = 118 \times J_{HNO_3}$	10
	(R8) $Deposited\_HNO_3/nitrate + hv \xrightarrow{J_{D\_HNO_3/nirate}} 0.67HONO + 0.33NO_2$	-	$J_{D\_HNO_3/nirate} = 48 \times J_{HNO_3}$	
Emission	Biomass Burning	-	FINNv1.5	11
	Traffic	-	Gasoline: $HONO_{traffic}/NO_x = 0.8\%$ Diesel: $HONO_{traffic}/NO_x = 2.3\%$	7
	Soil	-	$HONO_{soil}/NO_x = f$(soil water content)	12

1. Burkholder et al. (2015); 2. Burkholder et al. (2020); 3. Xue et al. (2022); 4. Czader et al. (2012); 5. Vandenboer et al. (2013); 6. Sarwar et al. (2008); 7. Zhang et al. (2016); 8. Yu et al. (2021); 9. Yu et al. (2022); 10. Fu et al. (2019); 11. Wiedinmyer et al. (2011); 12. Meusel et al. (2018)

2.3 HONO sources

In this study, we considered several possible missing HONO sources or processes in the CMAQ model simulations. The possible missing HONO sources include gas-phase HONO reactions, three HONO emission sources, three heterogeneous HONO reactions, and two photolytic reactions. The considered possible missing HONO sources are also contrasted to the current HONO processes embedded in the CMAQ v5.2.1 model in Table 1. The details of each HONO process are discussed below.

Table 2. Design for 8 EXP simulations.

HONO Source	Experiment							
	EXP1	EXP2	EXP3	EXP4	EXP5	EXP6	EXP7	EXP8
GAS[1)]	√	√	√	√	√	√	√	√
BioB[2)]		√	√	√	√	√	√	√
TRAF[3)]			√	√	√	√	√	√
SOIL[4)]				√	√	√	√	√
HET_A[5)]					√	√	√	√
HET_L[6)]						√	√	√
HET_BD[7)]							√	√
$RENO_x$[8)]								√

[1)] Gas-phase reactions; [2)] Biomass Burning Emissions; [3)] Traffic Emissions; [4)] Soil Emissions; [5)] Heterogeneous reactions on aerosol surfaces; [6)] Heterogeneous reactions on the surfaces of leaves; [7)] Heterogeneous reactions on the surfaces of buildings; [8)] Renoxification

2.3.1 Gas Phase reactions (GAS)

We used the SAPRC-07 TC chemical mechanism as base mechanism. A total of 4 gas-phase HONO-related reactions were considered for HONO formation and dissociation (Carter, 2010; Foley et al., 2010; Appel et al., 2016). HONO is produced by i) photolysis of nitrophenol (NPHE) (R2) and ii) reaction of NO with OH in the presence of the third body (M) (R3). Meanwhile, HONO is removed by reaction with OH radicals (R4) and photolytic dissociation (R1). All these reactions are shown below:

$$\mathrm{NPHE} + \mathrm{hv} \xrightarrow{j_{\mathrm{NPHE}}} \mathrm{HONO} + \mathrm{xPROD2} \quad \text{(R2)}$$

$$\mathrm{OH} + \mathrm{NO} + \mathrm{M} \xrightarrow{k_3} \mathrm{HONO} \quad \text{(R3)}$$

$$HONO + OH \xrightarrow{k_4} H_2O + NO_2 \quad (R4)$$

where, J_{NPHE} (R2) and J_{HONO} (R1) are the photolysis rates constants of NPHE and HONO, respectively, which were adopted from the study of Stockwell et al. (1990). As shown in Table 1, J_{NPHE} was calculated, based on J_{NO2} (i.e., $J_{NPHE} = 1.50 \times 10^{-3} \times J_{NO2}$), which was defined in Bejan et al. (2006). k_3 and k_4 are the reaction rate constants of (R3) and (R4) and were obtained from the National Aeronautics and Space Administration (NASA) Jet Propulsion Laboratory (JPL) Publication 19 (Burkholder et al., 2015). Among these reactions, the reaction rate constants of (R3) and (R4) were updated in our study (refer to Table 1). The effect of these gaseous reactions on HONO mixing ratios was tested in the EXP1 simulation (see GAS in Table 2).

2.3.2 Biomass burning emissions (BioB)

Biomass combustion includes three types of burning events: natural wildfires, agricultural fires, and wood burning (Wiedinmyer et al., 2011). In East Asia, agricultural fires typically occur in early summer and fall (Ryu et al., 2004; Tao et al., 2013; Zhang et al., 2013). The period of the KORUS-AQ campaign coincides with the period of the agricultural residue burning after barley and wheat harvest in East Asia. Biomass burning emissions, including agricultural fire emissions, were obtained from the Fire INventory from NCAR version 1.5 (FINN v1.5, Wiedinmyer et al., 2006; Wiedinmyer et al., 2011). This was then considered in the EXP2 simulation (see BioB in Table 2). The spatial distributions of HONO emissions from the biomass burning events in the East Asia domain (A1), South Korea domain (A2), and Seoul Metropolitan Area domain (A3) are presented in Fig. 1a and 1b. However, we found that the HONO emission rates used in the EXP2 simulation were relatively small, compared to the total HONO emission rates presented in Fig. 1 and Table 3.

Table 3. HONO emission rates from biomass burning, traffic, and soil. The total HONO emission rates during the period of the KORUS-AQ campaign are shown.

Region	Source			
	Biomass Burning Emission ($g \cdot s^{-1}$)	Traffic Emission ($Mg \cdot s^{-1}$)	Soil Emission ($Mg \cdot s^{-1}$)	Total ($Mg \cdot s^{-1}$)
East Asia (A1)	2.46	6.40	5.65	14.51
South Korea (A2)	0.00	0.32	0.06	0.38
Seoul Metropolitan Area (A3)	0.00	0.10	0.01	0.1

2.3.3 Traffic emissions (TRAF)

Traffic emissions are an important HONO source, particularly at night (Zhang et al., 2016). HONO is emitted directly from vehicle exhaust systems. In this study, to estimate the direct HONO emissions from traffic sources, we assumed that the HONO to NO_x emission ratio is 0.8% for gasoline vehicles and 2.3% for diesel vehicles (Zhang et al., 2016). All off-road vehicles were treated as diesel vehicles in the calculations of HONO emissions (Gutzwiller et al., 2002). Table 3 presents the total emission rates for East Asia, South Korea, and the Seoul Metropolitan Area, which are 6.40, 0.32, and 0.1 Mg s^{-1}, respectively. Moreover, as shown in Fig. 1c and 1d, HONO emissions from traffic sources are dominant, particularly in metropolitan areas such as Seoul, Beijing, Shanghai, and Hong Kong. The contribution of traffic sources to total HONO emissions was estimated to be dominant in the Seoul Metropolitan Area. In the EXP3 simulation, the impact of the traffic source (see TRAF in Table 2) on the atmospheric HONO mixing ratios was investigated.

2.3.4 Soil emissions (SOIL)

Emissions from soil bacterial activity are important sources of HONO. The amount of their emissions depends on the soil type, land category, fertilization, temperature, soil water

content (SWC in %), and soil pH (Meusel et al., 2018; Wu et al., 2020). In this study, HONO emissions were estimated based on the ratio of HONO to NO_x emissions from soil (Oswald et al., 2013). SWC was used as a proxy for soil pH due to the technical limitations of direct measurement of the soil pH. The SWCs were set at 0-7.5%, 7.5-15%, 15-20%, 20-30% and 30-40% for HONO-to-NO_x ratios of 1.0, 0.67, 0.75, 0.5 and 0.25, respectively, because the ratio of HONO to NO_x is very sensitive to the water content in the soil. For this estimation, monthly soil NO_x emissions were acquired from the MEGAN v2.10 model.

The HONO emission rate from soil was estimated at 0.06 Mg s^{-1} for South Korea, accounting for ~16% of the total HONO emission rate in South Korea (refer to Table 3). The spatial distributions of emission are presented in Fig. 1e and 1f. The impact of HONO soil emissions (see SOIL in Table 2) was examined in the EXP4 simulation.

2.3.5 Heterogeneous reaction of NO_2 on atmospheric aerosol surfaces (HET_A)

In the EXP5 simulation, we added the heterogeneous reaction of NO_2 on the surface of atmospheric aerosols via reaction (R5) (see HET_A in Table 2), which has been reported to be a possible pathway for HONO formation (Svensson et al., 1987; Wiesen et al., 1995; Reisinger, 2000; Han et al., 2017; Lu et al., 2018).

$$2NO_2 + H_2O \xrightarrow{k_{aerosol}} HONO + HNO_3 \quad \text{(R5)}$$

We found a similar diurnal pattern of the concentration ratio of HONO/NO_2 to the HONO mixing ratio at the Olympic Park station. This indicates that the conversion of NO_2 to HONO via reaction (R5) may be a main process for HONO formation (Fig. S2). The HONO/NO_2 ratios at the Olympic Park station in Seoul ranged from 1.9% to 6.8% during the KORUS-AQ campaign, which is also comparable to those observed in Taichung, Taiwan, and Shanghai, China (Tong et al., 2015; Hao et al., 2020).

The current AERO6 module in the CMAQv5.2.1 model already considers reaction (R5) but does not take into account 'photo-enhancement'. However, several previous studies suggested that the photo-enhanced reactions should produce more HONO molecules during the daytime (Li et al., 2010; Czader et al., 2012; Colussi et al., 2013; Levy et al., 2014; Fu et al., 2019). The potential photo-enhancement of the reaction (R5) was taken into account by making $k_{aerosol}$ dependent on the magnitude of light intensity:

$$k_{aerosol} = \frac{1}{4} \times v_{NO_2} \times \frac{S_{aero}}{V} \times \gamma_{a,NO_2} \quad \text{(Eq.1)}$$

$$\gamma_{a,NO_2} = 8.0 \times 10^{-6} \quad \text{(nighttime)}$$

$$\gamma_{a,NO_2} = 1.3 \times 10^{-4} \times \left(\frac{\text{light intensity}}{900}\right) \quad \text{(daytime)}$$

where, v_{NO_2}, $\frac{S_{aero}}{V}$, and γ_{a,NO_2} represent the mean molecular velocity of NO_2 ($m \cdot s^{-1}$), the aerosol surface density ($m^2 \cdot m^{-3}$), and the NO_2 uptake coefficient on the surface of atmospheric aerosols, respectively. The values of γ_{a,NO_2} were finally selected from the sensitivity tests. It should also be noted in Table 1 that the CMAQ v5.2.1 model simply uses a fixed reaction constant (= $10^{-4} \times \frac{S_{aero}}{V}$) for this heterogeneous reaction.

2.3.6 Heterogeneous reactions of NO_2 on tree leaf and building surfaces (HET_L and HET_BD)

The heterogeneous reaction of NO_2 can also take place on the ground surfaces (e.g., tree leaves and buildings). Several studies have reported that heterogeneous reactions on the surfaces of tree leaves and buildings via reaction (R6) can contribute to the HONO mixing ratios in the atmosphere (An et al., 2013; Karamchandani et al., 2015; Hou et al., 2016; Zhang et al., 2016). Therefore, we also considered these photo-enhanced heterogeneous NO_2 reactions.

$$2NO_2 + H_2O \xrightarrow{k_{L\&B}} HONO + HNO_3 \quad \text{(R6)}$$

In this study, $k_{L\&B}$ was calculated using equation (2), with a modification of the equation:

$$k_{L\&B} = \frac{1}{8} \times v_{NO_2} \times \gamma_{g,NO_2} \times \left(\frac{S_{g,building}}{V} + \frac{S_{g,leaf}}{V}\right) \quad \text{(Eq.2)}$$

$$\gamma_{g,NO_2} = 5.0 \times 10^{-7} \quad \text{(nighttime)}$$

$$\gamma_{g,NO_2} = 5.8 \times 10^{-6} \times \left(\frac{\text{light intensity}}{900}\right) \quad \text{(daytime)}$$

where γ_{g,NO_2} is the NO_2 uptake coefficient on the ground surfaces. These values are also selected from sensitivity tests. Here, $\frac{S_{g,building}}{V}$ represents the ratios of the building surface area to the volume, which were calculated from equation (3):

$$\frac{S_{g,building}}{V} = \text{PURB} \times \frac{0.3\frac{m^2}{m^3}}{100\%} \quad \text{(Eq.3)}$$

where, PURB represents the percentage of building area with a maximum value of 0.3 (Zhang et al., 2016). For vegetation areas, $\frac{S_{g,leaf}}{V}$ (the ratio of the leaf surface to volume) was estimated based on leaf area index (LAI) information, along with equation (4) proposed by Sarwar et al. (2008):

$$\frac{S_{g,leaf}}{V} = \frac{2 \times \text{LAI}}{H} \quad \text{(Eq.4)}$$

where, H represents the height of the first layer of the model simulation (Sarwar et al., 2008; Yuan et al., 2011; Zhang et al., 2012). The LAI was obtained from improved Moderate Resolution Spectroradiometer (MODIS) land use data (Yuan et al., 2011).

2.3.7. Photolysis reactions ($RENO_x$)

Several measurement studies have reported that the photolytic dissociation of particulate nitrate (pNO_3) in the atmosphere (R7) may be able to explain the high HONO mixing ratios observed during the daytime (Ye et al., 2017; Romer et al., 2018). Other studies suggested that the photolysis reactions of HNO_3 and nitrate deposited on tree canopies and artificial surfaces (R8) can also be significant sources of daytime HONO, particularly in rural areas (Zhou et al., 2011; Ye et al., 2016). All these heterogeneous reactions from N(V) to N(III) or N(IV) are called atmospheric ‘renoxification’. Some studies have also reported that these

316 types of reduction reactions actually take place in the snow (Chen et al., 2019). In order to
317 better estimate the daytime mixing ratios of HONO in the atmosphere, reactions (R7) and (R8)
318 were included in the EXP8 simulation (see $RENO_x$ in Table 2).

319 $$pNO_3 \xrightarrow{h\nu} 0.67\ HONO + 0.33\ NO_2 \quad \text{(R7)}$$

320 $$\text{deposited\_}HNO_3/\text{nitrate} \xrightarrow{h\nu} 0.67\ HONO + 0.33\ NO_2 \quad \text{(R8)}$$

321 In the EXP8 simulation, we chose equations for both the photolysis rate constant of particulate
322 NO_3^- (denoted by J_{pNO_3}) and the photolysis rate constant of HNO_3/nitrate deposited on
323 surfaces (denoted by $J_{D\_HNO_3/nitrate}$), following the methods proposed by Zhang et al. (2022),
324 and Fu et al. (2019). These equations are presented below:

325 $$J_{pNO_3} = 118 \times J_{HNO_3} \quad \text{(Eq.5)}$$

326 $$J_{D\_HNO_3/nirate} = 48 \times J_{HNO_3} \quad \text{(Eq.6)}$$

327 where, J_{HNO_3} is the reaction rate constant of gaseous HNO_3 photo-dissociation, which is
328 calculated by the photolysis rate preprocessor module (JPROC) in the CMAQ model.

329 **3. Results and Discussions**

330 In this section, we first evaluated the performances of the modified CMAQ models in
331 terms of HONO mixing ratios by comparing the model outputs with ground-based observations
332 from the Olympic Park station in South Korea. We then carried out sensitivity tests to estimate
333 the contributions of the various atmospheric HONO processes to atmospheric HONO mixing
334 ratios.

335 **3.1 Observed vs Simulated HONO mixing ratios**

336 Figure 2 presents the hourly variations of the HONO mixing ratios at the Olympic Park
337 station. Observations are marked with open black circles, and colored lines represent HONO
338 mixing ratios calculated from the 8 EXP simulations. When HONO sources were added

sequentially to the experiments, the HONO mixing ratios averaged over the entire simulation period increased from 0.06 ppb (EXP1 simulation) to 1.18 ppb (EXP8 simulation). The averaged HONO mixing ratios in the EXP8 simulation, which took into account all the HONO processes, were almost comparable to those observed from the ground (1.35 ppb of HONO).

The CMAQ-simulated HONO mixing ratios were particularly underestimated from 19 May to 23 May, 2016 (refer to gray-shadow period in Fig. 2). This period was characterized by low wind speeds and poor mixing within planetary boundary layer height (PBLH), which can lead to the accumulation of air pollutants (Crawford et al., 2021). On the other hand, the WRF model has a strong tendency to produce higher wind speeds than the actual ones, which may lead to underestimation of air pollutant concentrations (Jo et al., 2017). In particular, the modeled wind speed during the stagnant period is overestimated by 36.3% compared to the observed wind speed, which is significantly higher than the overestimation of 23.4% for the entire KORUS-AQ period. Therefore, the underestimation of the HONO mixing ratios may be caused by the overestimation of the wind speed on a given period. Despite all the discrepancies, the HONO mixing ratios agree relatively well with the observed HONO mixing ratios during the period of the KORUS-AQ campaign.

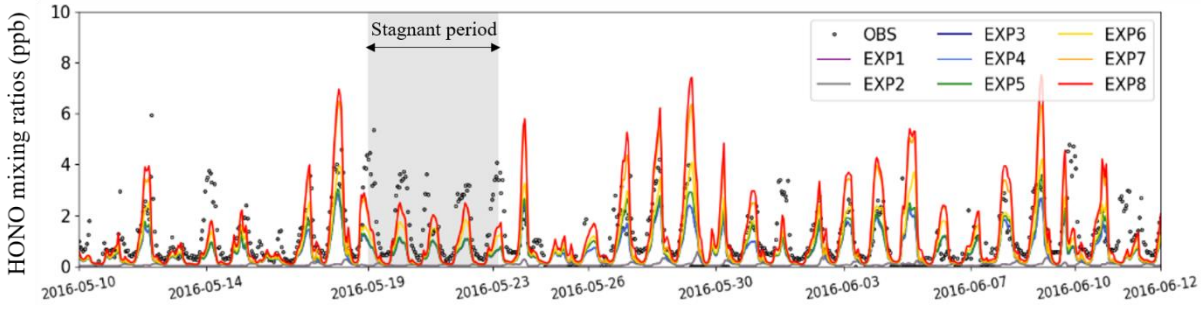

Figure 2. Hourly variations of the HONO mixing ratios (unit: ppb) at the Olympic Park station in Seoul. The observations are marked with black circles and the colored lines represent the HONO mixing ratios obtained from the 8 experimental simulations.

Figure 3 shows the diurnal variations of averaged HONO mixing ratios estimated from the 8 EXP simulations, together with HONO observations at the Olympic Park station. For the

analysis of Fig. 3, daytime and nighttime are defined as 06:00–18:00 and 18:00–06:00 local standard time, respectively. The EXP1 simulation showed slightly elevated HONO mixing ratios during the daytime (purple line in Fig. 3) due to the net production of HONO in the gas phase. The peak mixing ratio of the simulated HONO is ~0.14 ppb, which is significantly lower than the observed mixing ratio. The large differences between EXP1 results and observations suggest that there should be more unaccountable sources of HONO, which should be further taken into account in our model simulations.

In the EXP2 simulation, HONO emissions from biomass burning were added. Several studies have reported that direct and indirect sources emitted from biomass burning events could contribute to the primary/secondary HONO formation (Gen et al., 2021; Wang et al., 2021; Jiang et al., 2023). However, the addition of these biomass burning emissions resulted in nearly negligible impact on the HONO mixing ratios, because no major biomass-burning events occurred in South Korea during the period of the KORUS-AQ campaign (refer to Fig. 1b). Thus, there are minimal differences between the EXP1 and EXP2 simulations (i.e., between the purple and grey lines in Fig. 3).

EXP3 simulation was then carried out to examine the impact of traffic sources (TRAF) on HONO mixing ratios. The average HONO mixing ratio increases to ~0.55 ppb. As previously discussed in Fig. 1c, HONO emissions from traffic sources can be significant, particularly in the Seoul Metropolitan Area. However, simulated levels of HONO are still much lower than observed levels of HONO.

HONO emissions from soil (SOIL) were further included in the EXP4 simulation. As discussed previously, several studies have reported that the consideration of soil emissions can lead to large increases in atmospheric HONO mixing ratios, particularly in East Asia (Fig. 1e). However, it was found that almost no significant changes had occurred in South Korea. This is

385 because the low soil NO_x levels in the South Korea are linked to several factors: (i)
386 geographical feature mainly covered by forest and mountains areas; (ii) use of low nitrogen
387 fertilizers; (iii) the reduced availability of nitrogen in the soil caused by acidic deposition; and
388 (iv) the relatively high soil water content (SWC) over the Korean Peninsula (Kim et al., 2008;
389 An et al., 2023).

390 In the EXP5 simulation, the heterogeneous reactions of NO_2 on the surfaces of
391 atmospheric aerosols (HET_A) were further taken into account. The addition of these reactions
392 was found to have only minor effect on the HONO mixing ratios, because γ_{a,NO_2} used in Eq.
393 (1) is too small to enhance the HONO mixing ratios in reaction (R5). In our study, the
394 heterogeneous reactions on the surface of atmospheric aerosols contribute only ~0.06 ppb. The
395 heterogeneous reactions can be potentially important in more polluted regions where larger
396 aerosol surface areas are available (Zhang et al., 2019).

397 On the contrary, the HONO mixing ratios can be greatly enhanced by NO_2 to HONO
398 conversions on the surfaces of the tree leaves and buildings. These two processes were
399 implemented in the EXP6 and EXP7 simulations (HET_L and HET_BD). In these two cases,
400 there were significant increases in the HONO mixing ratios, particularly during the nighttime
401 (i.e., on average, increases of 0.23 and 0.55 ppb in the HONO mixing ratios were found in the
402 EXP6 and EXP7 simulations, respectively).

403 Finally, the photolytic renoxification of nitrate was added to the EXP8 simulation. In
404 this EXP8 simulation, the averaged HONO mixing ratios increased by 0.11 ppb. The
405 enhancement in the HONO mixing ratios was particularly large in the early morning (an
406 increase of ~0.23 ppb was found at 6 a.m.). Overall, the EXP8 simulation produced the best
407 HONO mixing ratios (averaged value of 1.18 ppb), compared to observed HONO mixing ratio
408 (1.35 ppb). Also, the estimated HONO mixing ratios were more comparable than those in the

CTRL (original CMAQ v5.2.1) model simulation (represented by black squares in Fig. 3). Again, it is noted that our simulations incorporated 'new HONO processes' such as: i) the photo-enhanced HONO production pathway through (R5) and (R6); ii) daytime HONO production from renoxification reactions through (R7) and (R8); and iii) HONO emissions (refer to Table 1).

In addition to the graphical comparison in Fig. 3, several statistical metrics were also calculated to evaluate the performances of the 8 EXP and CTRL simulations in Table 4. Significant improvements were found when the HONO processes were sequentially added from the EXP1 to the EXP8 simulations. For example, the index of agreement (IOA) increases from 0.44 to 0.76, and the mean bias (MB) decreases drastically from -1.29 ppb to -0.17 ppb from the EXP1 to the EXP8. In particular, the EXP8 simulation showed the best performance, compared to the CTRL simulation during the daytime. For example, the IOA during the daytime increased from 0.59 to 0.68, while the MB decreases from -0.57 to -0.34, respectively. The root mean square error (RMSE) also decreased from 0.80 to 0.70 during the daytime.

Although the EXP8 simulation showed a notable enhancement in HONO production, the HONO mixing ratios were still underestimated during the daytime. Such underestimation of HONO mixing ratios during the daytime could be attributed to stronger HONO photo-dissociation than in real situations. This is possibly due to failure in predicting cloud shades fractions in meteorological modeling and/or due to additional sources that were not considered in this study (e.g., acid displacement for HNO_3 and HCl, nitrate and Fe(II) in iron-organic complex under irradiation, and renoxification of nitrate in presence of carbonaceous aerosols) (Vandenboer et al., 2013; Gen et al., 2021; Wang et al., 2021). This certainly indicates that additional work is needed to further investigate HONO formation and removal during the daytime.

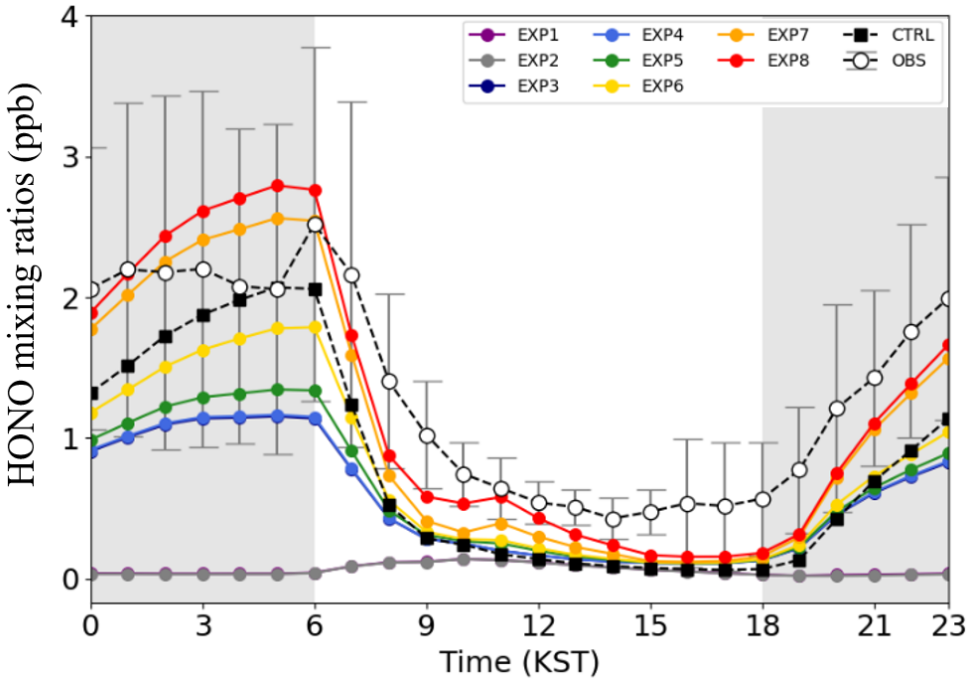

Figure 3. Diurnal variations of HONO mixing ratios (unit: ppb) at the Olympic Park station averaged over the period of the KORUS-AQ campaign. Error bars and grey-shaded areas indicate one standard deviation and nighttime (18 – 06 LST, Local Standard Time), respectively.

Table 4. Statistical analysis with modeled and observed HONO mixing ratios at the Olympic Park station, Seoul, Korea.

Experiment	Observed mean (ppb)	Modeled mean (ppb)	RMSE (ppb)	MB (ppb)	IOA
CTRL	1.35	0.78	1.06	-0.57	0.75
EXP1	1.35	0.06	1.68	-1.29	0.44
EXP2	1.35	0.06	1.68	-1.29	0.44
EXP3	1.35	0.55	1.15	-0.79	0.63
EXP4	1.35	0.56	1.15	-0.79	0.64
EXP5	1.35	0.61	1.12	-0.73	0.66
EXP6	1.35	0.75	1.02	-0.60	0.72
EXP7	1.35	1.07	1.05	-0.28	0.77
EXP8	1.35	1.18	1.12	-0.17	0.76

3.2 Relative contribution of HONO sources

Individual HONO processes affect the HONO mixing ratios in different ways. Figure 4 summarizes the relative contribution of HONO processes to the HONO mixing ratios. During the daytime, both GAS and $RENO_x$ contribute significantly to the production of atmospheric HONO molecules. In particular, the contribution of these two processes is the largest between 10:00 and 16:00 local time, when sunlight is strong. These two processes account for 29.1% and 29.8% of the daytime HONO production, respectively, but are almost negligible during the nighttime.

During the nighttime, TRAF (denoted by navy color in Fig. 4) contributes the large portion of 47.2% of the total HONO production. However, there is a possibility that TRAF might have been somewhat overestimated during the nighttime since we applied constant diurnal anthropogenic NO_x emissions, including those from traffic source. In turn, HET_BD and HET_L exhibit substantial contributions of 28.5% and 10.6%, respectively during the nighttime. The contributions of other processes such as biomass burning (BioB) and heterogeneous reactions on atmospheric aerosols (HET_A) are minimal. HET_A contributes only 4.3% during the nighttime. ~~Its contribution increases to 4.2% during the daytime.~~ In terms of the average 24-hour contribution, TRAF (41.4%), HET_BD (27.1%), and HET_L (11.1%) are the large sources of atmospheric HONO at the Olympic Park station.

Using the same approach, we analyzed the HONO source contributions across South Korea during the period of the KORUS-AQ campaign. As shown in Fig. 5f and 5c, HET_L and TRAF were modeled to have the largest impacts on HONO production, contributing 0.15 ppb (41.5%) and 0.08 ppb (18.1%), respectively, across South Korea (also, refer to the incremental ratio in Fig. S3).

Fig. 6 shows the contributions of different sources to the HONO mixing ratios at 8 super monitoring stations. As shown in Fig. 6, each station has different characteristics in terms

of source contribution. In particular, the contribution of HET_L at the Daejeon is 44.4%. Also, TRAF in Bulkwang, Olympic Park, Mt.Taehwa, Ulsan, and Gwangju have large contributions of 41.2%, 41.4%, 29.3%, 29.6%, and 40.5%, respectively. As for TRAF and HET_BD, their contributions are high only in densely populated cities (refer to Fig. 5c and 5g). On the other hand, the contributions of BioB, SOIL, HET_A, and $RENO_x$ sources were insignificant, as shown in Fig. 5b, 5d, 5e, and 5h.

Meanwhile, at the Bangnyung and Jeju stations, $RENO_x$ has the largest contribution of 70.4%, and 33.2%, respectively. This is because the amounts of NO_2 and HONO from direct emissions (BioB, TRAF, and SOIL) are relatively small. The Bangnyung and Jeju stations are located on remote and less populated islands.

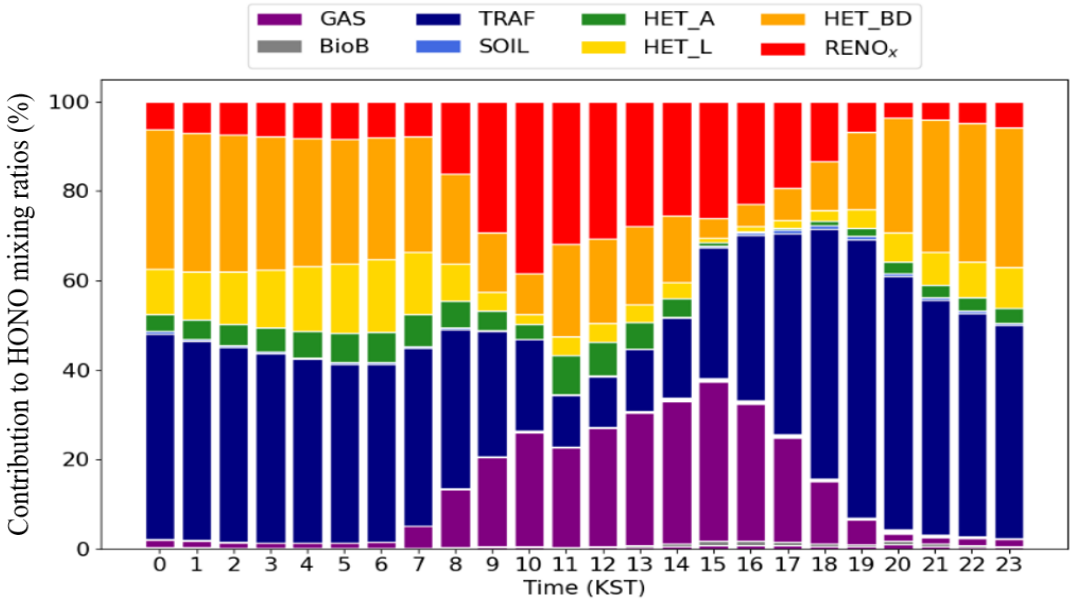

Figure 4. Diurnal contributions of individual HONO processes to the HONO mixing ratios at the Olympic Park station during the period of the KORUS-AQ campaign.

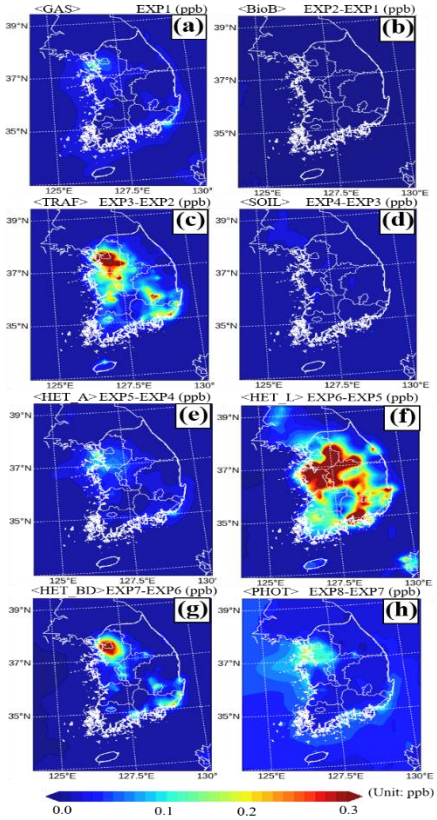

Figure 5. Spatial impacts of (a) gas phase reactions; (b) biomass burning emissions; (c) traffic emissions and (d) soil emissions; (e) heterogeneous reactions on the aerosol surfaces, (f) heterogeneous reactions on the leaf surfaces, and (g) heterogeneous reactions on the building surfaces; and (h) renoxification on HONO mixing ratios, based on model simulations during the period of the KORUS-AQ campaign in South Korea.

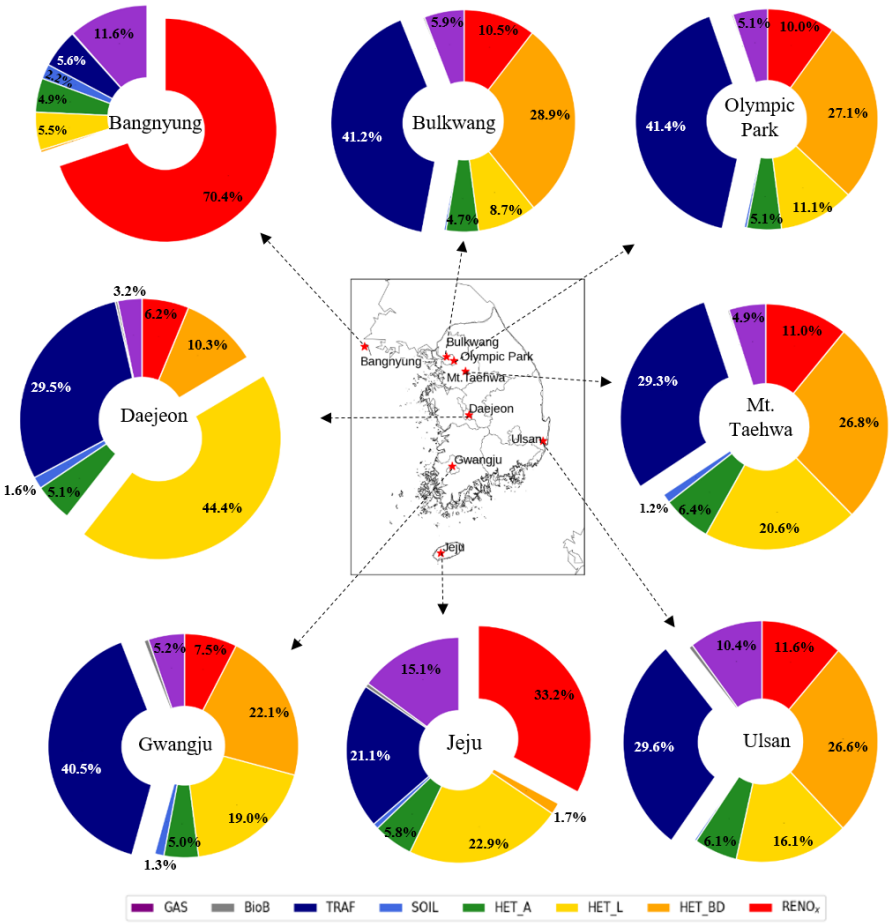

Figure 6. Contributions of individual processes to the average HONO mixing ratios at 8 monitoring stations during the period of the KORUS-AQ campaign.

3.3 Impact of HONO processes on atmospheric species

3.3.1 Impact on atmospheric species

We also investigated the effect of HONO processes on atmospheric levels of HO_x (=OH + HO_2), HCHO, O_3, NO, and $PM_{2.5}$ at the Olympic Park station. Figure 7 presents the diurnal concentrations of these gaseous and particulate species at the Olympic Park station. The mixing ratios of OH and HO_2 radicals in the EXP8 simulation increased by 0.02 ppt (35.2%) and 0.23 ppt (39.2%), respectively, compared to those in the CTRL simulation. This is certainly due to the enhancement in OH levels due to HONO photo-dissociation, and then HO_2 levels in the HO_x cycle. As shown in Fig. 7a (and 7b), the OH (and HO_2) mixing ratios increased from 0.21 ppt to 0.29 ppt (1.71 ppt to 2.28 ppt) at 1 p.m. local standard time. Subsequently, the

HCHO mixing ratios were also enhanced by 0.18 ppb (8.8%), due to increased VOC oxidation resulting from elevated levels of OH radicals (Fig. 7c). On the contrary, the NO mixing ratios in the EXP8 simulation decreased by 2.13 ppb (20.1%). This may be due to an increase in the mixing ratios of HO_2 and RO_2 radicals (organic peroxyl radicals) reacting with NO molecules (Fig. 7d). In other words, the reduced levels of NO indicate active NO to NO_2 conversion via $NO+HO_2$ and $NO+RO_2$ reactions. Such active NO to NO_2 conversion increases the mixing ratio of atmospheric ozone because these two reactions are rate-determining reactions for ozone production. This is presented in Fig. 7e. In Fig. 7e, the modeled ozone mixing ratios increased, approaching the observed ozone mixing ratios. This is another good result showing that the incorporation of atmospheric HONO processes may be able to enhance the accuracy of prediction of ozone mixing ratios. More details about ozone production are discussed in Sect. 3.3.2.

Elevated levels of atmospheric O_3 and HO_x can change the rates of particulate nitrate and sulfate production. In particular, the formation of particulate nitrates and sulfates can also be enhanced by increasing the levels of HNO_3, N_2O_5, and H_2SO_4. In addition, the nitrate concentration can also be enhanced by the HONO reaction (i.e., via $NO_2 + H_2O \rightarrow H^+ + NO_3^- + HONO$, as accounted for by R6) during the nighttime. In total, the addition of HONO processes increases $PM_{2.5}$ by 4.19 $\mu g\ m^{-3}$ (18.6%) at the Olympic Park station. However, $PM_{2.5}$ in the EXP8 simulation was still underestimated by 3.16 $\mu g\ m^{-3}$ at the Olympic Park station, as shown in Fig. 7f. There are several potential reasons for this underestimation, such as the underestimation of secondary organic aerosol (SOA) formation (e.g., Murphy et al., 2017). This issue may require further investigation in the future.

Figure S4 presents similar results for 320 AIR KOREA monitoring stations in South Korea. The impacts of HONO processes on atmospheric levels of OH, HO_2, O_3, and $PM_{2.5}$ are also presented in Fig. S5. Overall, we found that incorporating HONO chemistry into the

modeling system tends to enhance the mixing ratios of HO_x, which in turn increases the mixing ratios of O_3 and $PM_{2.5}$.

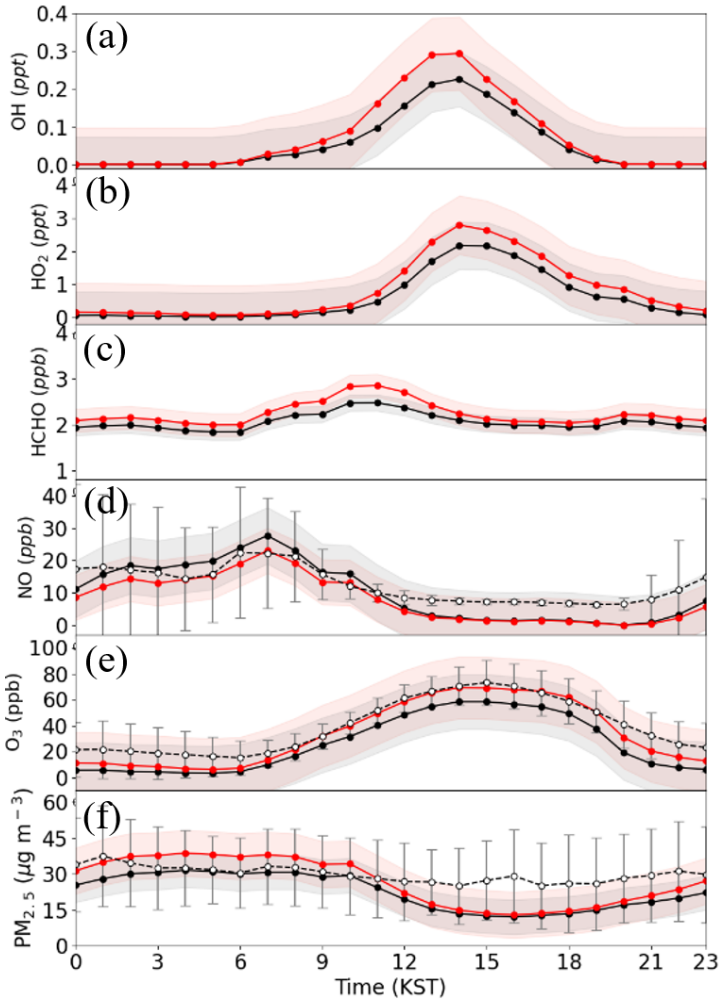

Figure 7. Diurnal variations of the mixing ratios of (a) OH, (b) HO_2, (c) HCHO, (d) NO, (e) O_3, and (f) $PM_{2.5}$ (black lines represent the mixing ratios from the CTRL simulation and the red lines represent those from the EXP8 simulation) and observations (marked with white open cycles) at the Olympic Park station during the period of the KORUS-AQ campaign. Shaded areas represent one standard deviation for each simulation.

3.3.2 Impact on net ozone production

The ozone mixing ratio is determined by the balance between ozone formation and destruction in the atmosphere. To better understand the impacts of HONO chemistry on ozone production, we quantitatively analyze the rate of net ozone production ($P(O_3)$). The $P(O_3)$ is defined by equation (7):

$$P(O_3) = F(O_3) - D(O_3) \quad \text{(Eq. 7)}$$

where, $F(O_3)$ and $D(O_3)$ represent the rate of ozone formation and destruction, respectively. $F(O_3)$ and $D(O_3)$ can be calculated from equations (8) and (9), respectively (Song et al., 2003; Mazzuca et al., 2016).

$$F(O_3) = k_{HO_2+NO}[HO_2][NO] + k_{RO_2+NO}[RO_2][NO] \quad \text{(Eq. 8)}$$

$$D(O_3) = k_{NO_2+OH}[NO_2][OH] + k_{O_3+VOC}[O_3][VOC] + k_{O(1D)+H_2O}[O(^1D)][H_2O] + k_{O_3+OH}[O_3][OH] + k_{O_3+HO_2}[O_3][HO_2] + k_{RO_2+NO_2}[RO_2][NO_2] + 2k_{NO_3+VOC}[NO_3][VOC] + 3k_{het}[N_2O_5] \quad \text{(Eq. 9)}$$

where k_i represents the reaction rate constants for each reaction i. In particular, k_{het} denotes the heterogeneous reaction rate constants of N_2O_5 radicals.

Figure 8a shows the diurnal variations of $F(O_3)$, $D(O_3)$, and $P(O_3)$ from the CTRL and EXP8 simulations. Including HONO processes in the EXP8 simulation resulted in an average $P(O_3)$ that was 10.6% higher than in the CTRL simulation. This is the primary reason for the ozone enhancement in Fig. 7e.

Figures 8b and 8c provide more details about the budget of ozone production. The main increase in $F(O_3)$ occurred through the reactions of HO_2 + NO and RO_2 + NO. On the other hand, the increase in $D(O_3)$ was mainly controlled by the NO_2 + OH reaction at the Olympic Park station. The increases in the HO_2 + NO and RO_2 + NO reaction rate exceeded the increases in the reaction rate of NO_2 + OH, leading to the net positive ozone production (i.e., positive $P(O_3)$) shown in Fig. 8a.

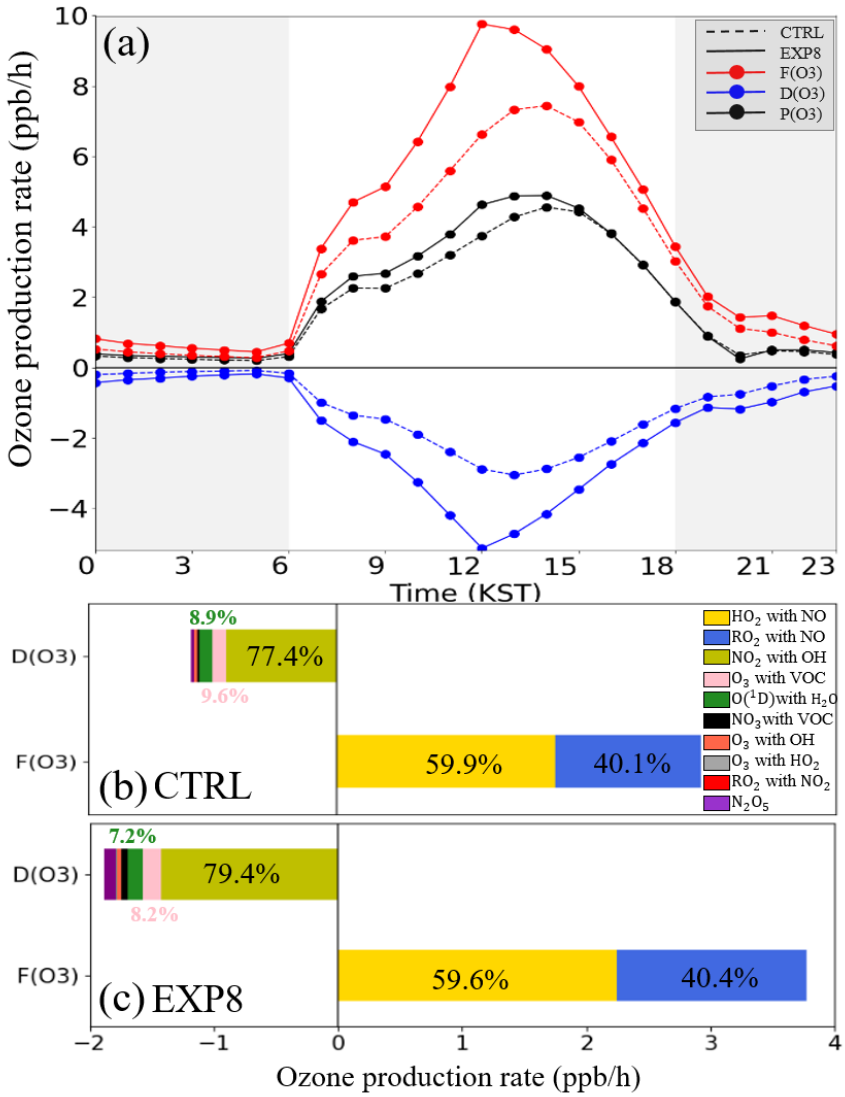

Figure 8. Diurnal variations of (a) net ozone production rate ($P(O_3)$; black line), ozone formation rate ($F(O_3)$; red line), and ozone loss rate ($D(O_3)$; blue line). The dashed and solid lines represent the CTRL and EXP8 simulations, respectively. Cumulative bar chart for $D(O_3)$ and $F(O_3)$ in case of (b) CTRL and (c) EXP8 simulations at the Olympic Park station during the period of the KORUS-AQ campaign.

4. Conclusions

In this study, we successfully incorporated the following HONO processes into the CMAQ modeling framework to enhance the accuracy in the predictions of HONO mixing ratios: i) gas-phase HONO reactions; ii) HONO emission from biomass burning; iii) HONO emission from traffic and soil; iv) photo-induced heterogeneous reactions on the surfaces of atmospheric aerosols, tree leaves, and buildings; and v) photolysis reactions of particulate

nitrate and deposited HNO_3/nitrate. The analysis showed that the incorporation of HONO processes into the CMAQ model framework increased the average HONO mixing ratios from 0.78 ppb to 1.18 ppb compared to the CTRL simulation. Average mixing ratios of HONO and its diurnal patterns became much more comparable to observations, with large improvements in statistical parameters. Especially during the daytime, IOA increased from 0.59 to 0.68, while the MB decreased from -0.57 ppb to -0.34 ppb, and RMSE dropped from 0.80 ppb to 0.70 ppb, as HONO processes were fully incorporated into the CMAQ model.

Several findings also emerged from the sensitivity simulations. First, each HONO process had a different effect on the HONO mixing ratios during the daytime and the nighttime at the Olympic Park station. For example, the GAS (29.1%) and $RENO_x$ processes (29.8%) had major contributions to the mixing ratios of HONO during the daytime, while the TRAF (47.2%) and HET_BD (28.5%) processes had large contributions to the mixing ratios of HONO during the nighttime. During the period of the KORUS-AQ campaign, HONO mixing ratios estimated at the Olympic Park station were enhanced by an average of 41.4% (TRAF), 27.1% (HET_BD), and 11.1% (HET_L).

In the experimental simulation including all the HONO processes (i.e., EXP8 simulation), the mixing ratios of OH, HO_2, HCHO, O_3, and $PM_{2.5}$ at the Olympic Park station increased by 0.02 ppt (35.2%), 0.23 ppt (39.2%), 0.18 ppb (8.8%), 7.86 ppb (30.8%), and 4.19 μg m^{-3} (18.6%), respectively, compared to those from the CTRL simulation. The net ozone production rate was enhanced by 0.19 ppb h^{-1} (10.6%) with the EXP8 simulation. This increases in $P(O_3)$ were caused mainly by the increased reaction rates of HO_2 + NO.

In this study, we improved our understanding of atmospheric HONO processes in South Korea. Nevertheless, we believe that both further field studies and modeling investigations are necessary for many remaining HONO-related issues such as NO_2 uptake

coefficient, possible missing HONO sources, and daytime photochemical reaction pathways of HONO. Such studies will also help to further improve the performances of current CTMs.

For example, the Airborne and Satellite Investigation of Asian Air Quality (ASIA-AQ) field campaign organized by the National Institute of Environmental Research (NIER) in Korea and the National Aeronautics and Space Administration (NASA) in the U.S. is planned in 2024 in South Korea. In this campaign, the HONO mixing ratios are scheduled to be measured in the aircraft and at the ground station. This joint campaign is thus expected to provide a valuable opportunity to expand our knowledge on atmospheric HONO processes and HONO photochemistry.

Code and data availability

After user registration, the WRF model 3.8.1 (https://www2.mmm.ucar.edu/wrf/users, last access: 11 April 2024) and CMAQ v5.2.1 (https://doi.org/10.5281/zenodo.1212601, last access: 11 April 2024) are available from web page. The observation data we used can be accessed at https://www-air.larc.nasa.gov/cgi-bin/ArcView/korusaq?GROUND-NIER-OLYMPIC-PARK=1 (last access: 11 April 2024).

Author contribution

KYK designed experiments and led manuscript writing and conceptualization. **KMH** and **CHS** supervised this project and contributed to experimental design and manuscript writing. **HJL, RB, JHY, GY,** and **BYK** performed research development. **JM** contributed to editing and writing review. **JHW** and **SJC** provided useful datasets.

Competing interests

Chul H. Song is a member of the editorial board of *Atmospheric Chemistry and Physics*. The authors declare that they have no conflict of interest.

Acknowledgement

This work was supported by the FRIEND (Fine Particle Research Initiative in East Asia Considering National Differences) Project through the National Research Foundation of Korea funded by the Ministry of Science and ICT (grant number: 2020M3G1A1114617). This work was also supported by the National Research Foundation of Korea (NRF) grand funded by the Korea government (MSIT) (grant number: 2021R1A2C1006660).

References

Acker, K., Möller, D., Wieprecht, W., Meixner, F. X., Bohn, B., Gilge, S., Plass-Dülmer, C., and Berresheim, H.: Strong daytime production of OH from HNO2 at a rural mountain site, Geophysical Research Letters, 33, https://doi.org/10.1029/2005GL024643, 2006.

Alicke, B., Geyer, A., Hofzumahaus, A., Holland, F., Konrad, S., Pätz, H., Schäfer, J., Stutz, J., Volz-Thomas, A., and Platt, U.: OH formation by HONO photolysis during the BERLIOZ experiment, Journal of Geophysical Research: Atmospheres, 108, PHO 3-1-PHO 3-17, https://doi.org/10.1029/2001JD000579, 2003.

An, J., Li, Y., Chen, Y., Li, J., Qu, Y., and Tang, Y.: Enhancements of major aerosol components due to additional HONO sources in the North China Plain and implications for visibility and haze, Advances in Atmospheric Sciences, 30, 57-66, https://doi.org/10.1007/s00376-012-2016-9, 2013.

An, Y., Shim, W., and Jeong, G.: High-Resolution Digital Soil Maps of Forest Soil Nitrogen across South Korea Using Three Machine Learning Algorithms, Forests, 14, 1141, https://doi.org/10.3390/f14061141, 2023.

Appel, K. W., Napelenok, S., Hogrefe, C., Pouliot, G., Foley, K. M., Roselle, S. J., Pleim, J. E., Bash, J., Pye, H. O., and Heath, N.: Overview and evaluation of the Community Multiscale Air Quality (CMAQ) modeling system version 5.2, International Technical Meeting on Air Pollution Modelling and its Application, 69-73, https://doi.org/10.1007/978-3-319-57645-9_11

Bejan, I., Abd El Aal, Y., Barnes, I., Benter, T., Bohn, B., Wiesen, P., and Kleffmann, J.: The photolysis of ortho-nitrophenols: a new gas phase source of HONO, Physical Chemistry Chemical Physics, 8, 2028-2035, https://doi.org/10.1039/B516590C, 2006.

Binkowski, F. S. and Roselle, S. J.: Models-3 Community Multiscale Air Quality (CMAQ) model aerosol component 1. Model description, Journal of geophysical research: Atmospheres, 108, https://doi.org/10.1029/2001JD001409, 2003.

Burkholder, J., Sander, S., Abbatt, J., Barker, J., Huie, R., Kolb, C., Kurylo, M., Orkin, V., Wilmouth, D., and Wine, P.: Chemical kinetics and photochemical data for use in atmospheric studies, evaluation no. 18, JPL publication 15-10; Jet Propulsion Laboratory, Pasadena, CA, Pasadena, http://jpldataeval.jpl.nasa.gov, 2015.

Byun, D. and Schere, K. L.: Review of the governing equations, computational algorithms, and other components of the Models-3 Community Multiscale Air Quality (CMAQ) modeling system, 2006.

Carter, W. P.: Development of the SAPRC-07 chemical mechanism, Atmospheric Environment, 44, 5324-5335, https://doi.org/10.1016/j.atmosenv.2010.01.026, 2010.

Chen, F. and Dudhia, J.: Coupling an advanced land surface–hydrology model with the Penn State–NCAR MM5 modeling system. Part I: Model implementation and sensitivity, Monthly weather review, 129, 569-585, https://doi.org/10.1175/1520-0493(2001)129<0569:CAALSH>2.0.CO;2, 2001.

Chen, Q., Edebeli, J., McNamara, S. M., Kulju, K. D., May, N. W., Bertman, S. B., Thanekar, S., Fuentes, J. D., and Pratt, K. A.: HONO, Particulate Nitrite, and Snow Nitrite at a Midlatitude Urban Site during Wintertime, ACS Earth and Space Chemistry, 3, 811-822, https://doi.org/10.1021/acsearthspacechem.9b00023, 2019.

Cheng, Z., Wang, S., Fu, X., Watson, J. G., Jiang, J., Fu, Q., Chen, C., Xu, B., Yu, J., and Chow, J. C.: Impact of biomass burning on haze pollution in the Yangtze River delta, China: a case study in summer 2011, Atmospheric Chemistry and Physics, 14, 4573-4585, https://doi.org/10.5194/acp-14-4573-2014, 2014.

Colussi, A. J., Enami, S., Yabushita, A., Hoffmann, M. R., Liu, W.-G., Mishra, H., and Goddard III, W. A.: Tropospheric aerosol as a reactive intermediate, Faraday Discussions, 165, 407-420, https://doi.org/10.1039/C3FD00040K, 2013.

Crawford, J. H., Ahn, J.-Y., Al-Saadi, J., Chang, L., Emmons, L. K., Kim, J., Lee, G., Park, J.-H., Park, R. J., Woo, J. H., Song, C.-K., Hong, J.-H., Hong, Y.-D., Lefer, B. L., Lee, M., Lee, T., Kim, S., Min, K.-E., Yum, S. S., Shin, H. J., Kim, Y.-W., Choi, J.-S., Park, J.-S., Szykman, J. J., Long, R. W., Jordan, C. E., Simpson, I. J., Fried, A., Dibb, J. E., Cho, S., and Kim, Y. P.: The Korea– United States Air Quality (KORUS-AQ) field study, Elementa, 9, 00163, https://doi.org/10.1525/elementa.2020.00163, 2021.

Crutzen, P. J. and Andreae, M. O.: Biomass burning in the tropics: Impact on atmospheric chemistry and biogeochemical cycles, Science, 250, 1669-1678, DOI: 10.1126/science.250.4988.1669, 1990.

Czader, B., Rappenglück, B., Percell, P., Byun, D., Ngan, F., and Kim, S.: Modeling nitrous acid and its impact on ozone and hydroxyl radical during the Texas Air Quality Study 2006, Atmospheric Chemistry & Physics Discussions, 12, https://doi.org/10.5194/acp-12-6939-2012,2012.

Czader, B. H., Choi, Y., Li, X., Alvarez, S., and Lefer, B.: Impact of updated traffic emissions on HONO mixing ratios simulated for urban site in Houston, Texas, Atmospheric Chemistry and Physics, 15, 1253, https://doi.org/10.5194/acp-15-1253-2015, 2015.

Foley, K., Roselle, S., Appel, K., Bhave, P., Pleim, J., Otte, T., Mathur, R., Sarwar, G., Young, J., and Gilliam, R.: Incremental testing of the Community Multiscale Air Quality (CMAQ) modeling system version 4.7, Geoscientific Model Development, 3, 205, https://doi.org/10.5194/gmd-3-205-2010, 2010.

Fu, X., Wang, T., Zhang, L., Li, Q., Wang, Z., Xia, M., Yun, H., Wang, W., Yu, C., Yue, D., Zhou, Y., Zheng, J., and Han, R.: The significant contribution of HONO to secondary pollutants during a severe winter pollution event in southern China, Atmos. Chem. Phys., 19, 1–14, https://doi.org/10.5194/acp-19-1-2019, 2019.

Gen, M., Zhang, R., and Chan, C. K.: Nitrite/nitrous acid generation from the reaction of nitrate and Fe (II) Promoted by photolysis of iron–organic complexes, Environmental Science & Technology, 55, 15715-15723, https://doi.org/10.1021/acs.est.1c05641, 2021.

Gligorovski, S.: Nitrous acid (HONO): An emerging indoor pollutant, Journal of Photochemistry and Photobiology A: Chemistry, 314, 1-5, https://doi.org/10.1016/j.jphotochem.2015.06.008, 2016.

Grell, G. A. and Freitas, S. R.: A scale and aerosol aware stochastic convective parameterization for weather and air quality modeling, Atmos. Chem. Phys, 14, 5233-5250, https://doi.org/10.5194/acp-14-5233-2014, 2014.

Guenther, A. B., Jiang, X., Heald, C. L., Sakulyanontvittaya, T., Duhl, T., Emmons, L. K., and Wang, X.: The Model of Emissions of Gases and Aerosols from Nature version 2.1 (MEGAN2.1): an extended and updated framework for modeling biogenic emissions, Geosci. Model Dev., 5, 1471–1492, https://doi.org/10.5194/gmd-5-1471-2012, 2012.

Gutzwiller, L., Arens, F., Baltensperger, U., Gäggeler, H. W., and Ammann, M.: Significance of semivolatile diesel exhaust organics for secondary HONO formation, Environmental science & technology, 36, 677-682, https://doi.org/10.1021/es015673b, 2002.

Han, C., Yang, W., Yang, H., and Xue, X.: Enhanced photochemical conversion of NO2 to HONO on humic acids in the presence of benzophenone, Environmental Pollution, 231, 979-986, https://doi.org/10.1016/j.envpol.2017.08.107, 2017.

Hao, Q., Jiang, N., Zhang, R., Yang, L., and Li, S.: Characteristics, sources, and reactions of nitrous acid during winter at an urban site in the Central Plains Economic Region in China, Atmospheric Chemistry and Physics, 20, 7087-7102, https://doi.org/10.5194/acp-20-7087-2020, 2020.

Harris, G. W., Carter, W. P., Winer, A. M., Pitts, J. N., Platt, U., and Perner, D.: Observations of nitrous acid in the Los Angeles atmosphere and implications for predictions of ozone-precursor relationships, Environmental science & technology, 16, 414-419, https://doi.org/10.1021/es00101a009, 1982.

Hendrick, F., Müller, J.-F., Clémer, K., Wang, P., De Mazière, M., Fayt, C., Gielen, C., Hermans, C., Ma, J. Z., Pinardi, G., Stavrakou, T., Vlemmix, T., and Van Roozendael, M.: Four years of ground-based MAX-DOAS observations of HONO and NO_2 in the Beijing area, Atmos. Chem. Phys., 14, 765–781, https://doi.org/10.5194/acp-14-765-2014, 2014.

Hong, S.-Y. and Lim, J.-O. J.: The WRF single-moment 6-class microphysics scheme (WSM6), Asia-Pacific Journal of Atmospheric Sciences, 42, 129-151, 2006.

Hong, S.-Y., Noh, Y., and Dudhia, J.: A new vertical diffusion package with an explicit treatment of entrainment processes, Monthly weather review, 134, 2318-2341, https://doi.org/10.1175/MWR3199.1, 2006.

Hou, S., Tong, S., Ge, M., and An, J.: Comparison of atmospheric nitrous acid during severe haze and clean periods in Beijing, China, Atmospheric environment, 124, 199-206, https://doi.org/10.1016/j.atmosenv.2015.06.023, 2016.

Hutzell, W., Luecken, D., Appel, K., and Carter, W.: Interpreting predictions from the SAPRC07 mechanism based on regional and continental simulations, Atmospheric Environment, 46, 417-429, https://doi.org/10.1016/j.atmosenv.2011.09.030, 2012.

Iacono, M. J., Delamere, J. S., Mlawer, E. J., Shephard, M. W., Clough, S. A., and Collins, W. D.: Radiative forcing by long-lived greenhouse gases: Calculations with the AER radiative transfer models, Journal of Geophysical Research: Atmospheres, 113, https://doi.org/10.1029/2008JD009944, 2008.

Jia, C., Tong, S., Zhang, W., Zhang, X., Li, W., Wang, Z., Wang, L., Liu, Z., Hu, B., and Zhao, P.: Pollution characteristics and potential sources of nitrous acid (HONO) in early autumn 2018 of Beijing, Science of The Total Environment, 735, 139317, https://doi.org/10.1016/j.scitotenv.2020.139317, 2020.

Jiang, H., Bao, F., Wang, J., Chen, J., Zhu, Y., Huang, D., Chen, C., and Zhao, J.: Direct formation of electronic excited NO2 contributes to the high yield of HONO during photosensitized renoxification, Environmental Science & Technology, 57, 11144-11151, https://doi.org/10.1021/acs.est.3c01342, 2023.

Jiménez, P. A., Dudhia, J., González-Rouco, J. F., Navarro, J., Montávez, J. P., and García-Bustamante, E.: A revised scheme for the WRF surface layer formulation, Monthly Weather Review, 140, 898-918, https://doi.org/10.1175/MWR-D-11-00056.1, 2012.

Jo, Y. J., Lee, H. J., Chang, L. S., and Kim, C. H.: Sensitivity study of the initial meteorological fields on the PM10 concentration predictions using CMAQ modeling, J. Korean Soc. Atmos. Environ., 33, 554–569, https://doi.org/10.5572/kosae.2017.33.6.554, 2017.

Karamchandani, P., Emery, C., Yarwood, G., Lefer, B., Stutz, J., Couzo, E., and Vizuete, W.: Implementation and refinement of a surface model for heterogeneous HONO formation in a 3-D chemical transport model, Atmospheric Environment, 112, 356-368, https://doi.org/10.1016/j.atmosenv.2015.01.046, 2015.

Keywood, M., Selleck, P., Reisen, F., Cohen, D., Chambers, S., Cheng, M., Cope, M., Crumeyrolle, S., Dunne, E., Emmerson, K., Fedele, R., Galbally, I., Gillett, R., Griffiths, A., Guerette, E.-A., Harnwell, J., Humphries, R., Lawson, S., Miljevic, B., Molloy, S., Powell, J., Simmons, J., Ristovski, Z., and Ward, J.: Comprehensive aerosol and gas data set from the Sydney Particle Study, Earth Syst. Sci. Data, 11, 1883–1903, https://doi.org/10.5194/essd-11-1883-2019, 2019.

Kim, C.-H., Park, I.-S., Kim, S.-K., Son, H.-Y., Lee, J.-J., Lee, J.-B., Song, C.-K., and Shim, J.-M.: Estimation and mapping of nitrogen uptake by forest in South Korea, Water, air, and soil pollution, 187, 315-325, https://doi.org/10.1007/s11270-007-9519-5, 2008.

Kim, S., VandenBoer, T. C., Young, C. J., Riedel, T. P., Thornton, J. A., Swarthout, B., Sive, B., Lerner, B., Gilman, J. B., and Warneke, C.: The primary and recycling sources of OH during the NACHTT-2011 campaign: HONO as an important OH primary source in the wintertime, Journal of Geophysical Research: Atmospheres, 119, 6886-6896, https://doi.org/10.1002/2013JD019784, 2014.

Kirchstetter, T. W., Harley, R. A., and Littlejohn, D.: Measurement of nitrous acid in motor vehicle exhaust, Environmental science & technology, 30, 2843-2849, https://doi.org/10.1021/es960135y, 1996.

Kleffmann, J., Gavriloaiei, T., Hofzumahaus, A., Holland, F., Koppmann, R., Rupp, L., Schlosser, E., Siese, M., and Wahner, A.: Daytime formation of nitrous acid: A major source of OH radicals in a forest, Geophysical Research Letters, 32, https://doi.org/10.1029/2005GL022524, 2005.

Kurtenbach, R., Becker, K., Gomes, J., Kleffmann, J., Lörzer, J., Spittler, M., Wiesen, P., Ackermann, R., Geyer, A., and Platt, U.: Investigations of emissions and heterogeneous formation of HONO in a road traffic tunnel, Atmospheric Environment, 35, 3385-3394, https://doi.org/10.1016/S1352-2310(01)00138-8, 2001.

Lee, J. D., Whalley, L. K., Heard, D. E., Stone, D., Dunmore, R. E., Hamilton, J. F., Young, D. E., Allan, J. D., Laufs, S., and Kleffmann, J.: Detailed budget analysis of HONO in central London reveals a missing daytime source, Atmos. Chem. Phys., 16, 2747–2764, https://doi.org/10.5194/acp-16-2747-2016, 2016.

Levy, M., Zhang, R., Zheng, J., Zhang, A. L., Xu, W., Gomez-Hernandez, M., Wang, Y., and Olaguer, E.: Measurements of nitrous acid (HONO) using ion drift-chemical ionization mass spectrometry during the 2009 SHARP field campaign, Atmospheric Environment, 94, 231-240, https://doi.org/10.1016/j.atmosenv.2014.05.024, 2014.

Li, D., Xue, L., Wen, L., Wang, X., Chen, T., Mellouki, A., Chen, J., and Wang, W.: Characteristics and sources of nitrous acid in an urban atmosphere of northern China: Results from 1-yr continuous observations, Atmospheric Environment, 182, 296-306, https://doi.org/10.1016/j.atmosenv.2018.03.033, 2018.

Li, G., Lei, W., Zavala, M., Volkamer, R., Dusanter, S., Stevens, P., and Molina, L. T.: Impacts of HONO sources on the photochemistry in Mexico City during the MCMA-2006/MILAGO Campaign, Atmos. Chem. Phys., 10, 6551–6567, https://doi.org/10.5194/acp-10-6551-2010, 2010.

Li, X., Brauers, T., Häseler, R., Bohn, B., Fuchs, H., Hofzumahaus, A., Holland, F., Lou, S., Lu, K. D., Rohrer, F., Hu, M., Zeng, L. M., Zhang, Y. H., Garland, R. M., Su, H., Nowak, A., Wiedensohler, A., Takegawa, N., Shao, M., and Wahner, A.: Exploring the atmospheric chemistry of nitrous acid (HONO) at a rural site in Southern China, Atmos. Chem. Phys., 12, 1497–1513, https://doi.org/10.5194/acp-12-1497-2012, 2012.

Li, X., Rohrer, F., Hofzumahaus, A., Brauers, T., Häseler, R., Bohn, B., Broch, S., Fuchs, H., Gomm, S., and Holland, F.: Missing gas-phase source of HONO inferred from Zeppelin measurements in the troposphere, Science, 344, 292-296, https://doi.org/10.1126/science.1248999 2014.

Lu, X., Wang, Y., Li, J., Shen, L., and Fung, J. C.: Evidence of heterogeneous HONO formation from aerosols and the regional photochemical impact of this HONO source, Environmental Research Letters, 13, 114002, https://doi.org/10.1088/1748-9326/aae492, 2018.

Mazzuca, G. M., Ren, X., Loughner, C. P., Estes, M., Crawford, J. H., Pickering, K. E., Weinheimer, A. J., and Dickerson, R. R.: Ozone production and its sensitivity to NO_x and VOCs: results from the DISCOVER-AQ field experiment, Houston 2013, Atmos. Chem. Phys., 16, 14463–14474, https://doi.org/10.5194/acp-16-14463-2016, 2016.

Meusel, H., Kuhn, U., Reiffs, A., Mallik, C., Harder, H., Martinez, M., Schuladen, J., Bohn, B., Parchatka, U., Crowley, J. N., Fischer, H., Tomsche, L., Novelli, A., Hoffmann, T., Janssen, R. H. H., Hartogensis, O., Pikridas, M., Vrekoussis, M., Bourtsoukidis, E., Weber, B., Lelieveld, J., Williams, J., Pöschl, U., Cheng, Y., and Su, H.: Daytime formation of nitrous acid at a coastal remote site in Cyprus indicating a common ground source of atmospheric HONO and NO, Atmos. Chem. Phys., 16, 14475–14493, https://doi.org/10.5194/acp-16-14475-2016, 2016.

Meusel, H., Tamm, A., Kuhn, U., Wu, D., Leifke, A. L., Fiedler, S., Ruckteschler, N., Yordanova, P., Lang-Yona, N., Pöhlker, M., Lelieveld, J., Hoffmann, T., Pöschl, U., Su, H., Weber, B., and Cheng, Y.: Emission of nitrous acid from soil and biological soil crusts represents an important source of HONO in the remote atmosphere in Cyprus, Atmos. Chem. Phys., 18, 799–813, https://doi.org/10.5194/acp-18-799-2018, 2018.

Monks, P. S., Granier, C., Fuzzi, S., Stohl, A., Williams, M. L., Akimoto, H., Amann, M., Baklanov, A., Baltensperger, U., and Bey, I.: Atmospheric composition change–global and regional air quality, Atmospheric environment, 43, 5268-5350, https://doi.org/10.1016/j.atmosenv.2009.08.021, 2009.

Murphy, B. N., Woody, M. C., Jimenez, J. L., Carlton, A. M. G., Hayes, P. L., Liu, S., Ng, N. L., Russell, L. M., Setyan, A., Xu, L., Young, J., Zaveri, R. A., Zhang, Q., and Pye, H. O. T.: Semivolatile POA and parameterized total combustion SOA in CMAQv5.2: impacts on source strength and partitioning, Atmos. Chem. Phys., 17, 11107–11133, https://doi.org/10.5194/acp-17-11107-2017, 2017.

Nagai, K. and Kubota, M.: On the volatilization of nitrogen during nitrification in soils under vinyl covered culture. 5. on the effects of iron complex salts and treatments with nitrates or chloride on volatilization of nitrous acid, Jap J Sci Soil and Manure, 1972.

Nakashima, Y. and Kajii, Y.: Determination of nitrous acid emission factors from a gasoline vehicle using a chassis dynamometer combined with incoherent broadband cavity-enhanced absorption spectroscopy, Science of The Total Environment, 575, 287-293, https://doi.org/10.1016/j.scitotenv.2016.10.050, 2017.

Nie, W., Ding, A. J., Xie, Y. N., Xu, Z., Mao, H., Kerminen, V.-M., Zheng, L. F., Qi, X. M., Huang, X., Yang, X.-Q., Sun, J. N., Herrmann, E., Petäjä, T., Kulmala, M., and Fu, C. B.: Influence of biomass burning plumes on HONO chemistry in eastern China, Atmos. Chem. Phys., 15, 1147–1159, https://doi.org/10.5194/acp-15-1147-2015, 2015.

Oswald, R., Behrendt, T., Ermel, M., Wu, D., Su, H., Cheng, Y., Breuninger, C., Moravek, A., Mougin, E., and Delon, C.: HONO emissions from soil bacteria as a major source of atmospheric reactive nitrogen, Science, 341, 1233-1235, https://doi.org/10.1126/science.1242266, 2013.

Pathak, R. K., Wu, W. S., and Wang, T.: Summertime $PM_{2.5}$ ionic species in four major cities of China: nitrate formation in an ammonia-deficient atmosphere, Atmos. Chem. Phys., 9, 1711–1722, https://doi.org/10.5194/acp-9-1711-2009, 2009.

Rappenglück, B., Lubertino, G., Alvarez, S., Golovko, J., Czader, B., and Ackermann, L.: Radical precursors and related species from traffic as observed and modeled at an urban highway junction, Journal of the Air & Waste Management Association, 63, 1270-1286, https://doi.org/10.1080/10962247.2013.822438, 2013.

Reisinger, A. R.: Observations of HNO2 in the polluted winter atmosphere: possible heterogeneous production on aerosols, Atmospheric Environment, 34, 3865-3874, https://doi.org/10.1016/S1352-2310(00)00179-5, 2000.

Ren, X., Harder, H., Martinez, M., Lesher, R. L., Oliger, A., Simpas, J. B., Brune, W. H., Schwab, J. J., Demerjian, K. L., and He, Y.: OH and HO2 chemistry in the urban atmosphere of New York City, Atmospheric Environment, 37, 3639-3651, https://doi.org/10.1016/S1352-2310(03)00459-X, 2003.

Romer, P. S., Wooldridge, P. J., Crounse, J. D., Kim, M. J., Wennberg, P. O., Dibb, J. E., Scheuer, E., Blake, D. R., Meinardi, S., and Brosius, A. L.: Constraints on Aerosol Nitrate Photolysis as a Potential Source of HONO and NOx, Environmental science & technology, 52, 13738-13746, https://doi.org/10.1021/acs.est.8b03861, 2018.

Ryu, S. Y., Kim, J. E., Zhuanshi, H., Kim, Y. J., and Kang, G. U.: Chemical composition of post-harvest biomass burning aerosols in Gwangju, Korea, Journal of the Air & Waste Management Association, 54, 1124-1137, https://doi.org/10.1080/10473289.2004.10471018, 2004.

Sarwar, G., Roselle, S. J., Mathur, R., Appel, W., Dennis, R. L., and Vogel, B.: A comparison of CMAQ HONO predictions with observations from the Northeast Oxidant and Particle Study, Atmospheric Environment, 42, 5760-5770, https://doi.org/10.1016/j.atmosenv.2007.12.065, 2008.

Skamarock, W. C., Klemp, J. B., Dudhia, J., Gill, D. O., Barker, D. M., Duda, M. G., Huang, X.-Y., Wang, W., and Powers, J. G.: G.: A description of the Advanced Research WRF version 3, NCAR Tech. Note NCAR/TN-475+ STR, 2008.

Song, C., Chen, G., Hanna, S., Crawford, J., and Davis, D.: Dispersion and chemical evolution of ship plumes in the marine boundary layer: Investigation of O3/NOy/HOx chemistry, Journal of Geophysical Research: Atmospheres, 108, https://doi.org/10.1029/2002JD002216, 2003.

Stockwell, W. R., Middleton, P., Chang, J. S., and Tang, X.: The second generation regional acid deposition model chemical mechanism for regional air quality modeling, Journal of Geophysical Research: Atmospheres, 95, 16343-16367, https://doi.org/10.1029/JD095iD10p16343, 1990.

Su, H., Cheng, Y. F., Cheng, P., Zhang, Y. H., Dong, S., Zeng, L. M., Wang, X., Slanina, J., Shao, M., and Wiedensohler, A.: Observation of nighttime nitrous acid (HONO) formation at a non-urban site during PRIDE-PRD2004 in China, Atmospheric Environment, 42, 6219-6232, https://doi.org/10.1016/j.atmosenv.2008.04.006, 2008.

Svensson, R., Ljungström, E., and Lindqvist, O.: Kinetics of the reaction between nitrogen dioxide and water vapour, Atmospheric Environment (1967), 21, 1529-1539, https://doi.org/10.1016/0004-6981(87)90315-5, 1987.

Tao, M., Chen, L., Wang, Z., Tao, J., and Su, L.: Satellite observation of abnormal yellow haze clouds over East China during summer agricultural burning season, Atmospheric environment, 79, 632-640, https://doi.org/10.1016/j.atmosenv.2013.07.033, 2013.

Tong, S., Hou, S., Zhang, Y., Chu, B., Liu, Y., He, H., Zhao, P., and Ge, M.: Comparisons of measured nitrous acid (HONO) concentrations in a pollution period at urban and suburban Beijing, in autumn of 2014, Science China Chemistry, 58, 1393-1402, https://doi.org/10.1007/s11426-015-5454-2, 2015.

VandenBoer, T. C., Brown, S. S., Murphy, J. G., Keene, W. C., Young, C. J., Pszenny, A., Kim, S., Warneke, C., de Gouw, J. A., and Maben, J. R.: Understanding the role of the ground surface in HONO vertical structure: High resolution vertical profiles during NACHTT-11, Journal of Geophysical Research: Atmospheres, 118, 10,155-110,171, https://doi.org/10.1002/jgrd.50721, 2013.

Wang, Y., Huang, D. D., Huang, W., Liu, B., Chen, Q., Huang, R., Gen, M., Mabato, B. R. G., Chan, C. K., and Li, X.: Enhanced nitrite production from the aqueous photolysis of nitrate in the presence of vanillic acid and implications for the roles of light-absorbing organics, Environmental Science & Technology, 55, 15694-15704, https://doi.org/10.1021/acs.est.1c04642, 2021.

Weber, B., Wu, D., Tamm, A., Ruckteschler, N., Rodriguez-Caballero, E., Steinkamp, J., Meusel, H., Elbert, W., Behrendt, T., and Soergel, M.: Biological soil crusts accelerate the nitrogen cycle through large NO and HONO

emissions in drylands, Proceedings of the National Academy of Sciences, 112, 15384-15389, https://doi.org/10.1073/pnas.1515818112, 2015.
Wiedinmyer, C., Akagi, S. K., Yokelson, R. J., Emmons, L. K., Al-Saadi, J. A., Orlando, J. J., and Soja, A. J.: The Fire INventory from NCAR (FINN): a high resolution global model to estimate the emissions from open burning, Geosci. Model Dev., 4, 625–641, https://doi.org/10.5194/gmd-4-625-2011, 2011.
Wiedinmyer, C., Quayle, B., Geron, C., Belote, A., McKenzie, D., Zhang, X., O'Neill, S., and Wynne, K. K.: Estimating emissions from fires in North America for air quality modeling, Atmospheric Environment, 40, 3419-3432, https://doi.org/10.1016/j.atmosenv.2006.02.010, 2006.
Wiesen, P., Kleffmann, J., Kurtenbach, R., and Becker, K. H.: Mechanistic study of the heterogeneous conversion of NO 2 into HONO and N 2 O on acid surfaces, Faraday Discussions, 100, 121-127, https://doi.org/10.1039/FD9950000121, 1995.
Woo, J.-H., Kim, Y., Kim, H.-K., Choi, K.-C., Eum, J.-H., Lee, J.-B., Lim, J.-H., Kim, J., and Seong, M.: Development of the CREATE Inventory in Support of Integrated Climate and Air Quality Modeling for Asia, Sustainability, 12, 7930, https://doi.org/10.3390/su12197930, 2020.
Woo, J.-H., Choi, K.-C., Kim, H. K., Baek, B. H., Jang, M., Eum, J.-H., Song, C. H., Ma, Y.-I., Sunwoo, Y., and Chang, L.-S.: Development of an anthropogenic emissions processing system for Asia using SMOKE, Atmospheric environment, 58, 5-13, https://doi.org/10.1016/j.atmosenv.2011.10.042, 2012.
WU, D., DENG, L., LIU, Y., XI, D., ZOU, H., WANG, R., SHA, Z., PAN, Y., HOU, L., and LIU, M.: Comparisons of the effects of different drying methods on soil nitrogen fractions: Insights into emissions of reactive nitrogen gases (HONO and NO), Atmospheric and Oceanic Science Letters, 13, 224-231, https://doi.org/10.1080/16742834.2020.1733388, 2020.
Xu, Z., Liu, Y., Nie, W., Sun, P., Chi, X., and Ding, A.: Evaluating the measurement interference of wet rotating-denuder–ion chromatography in measuring atmospheric HONO in a highly polluted area, Atmos. Meas. Tech., 12, 6737–6748, https://doi.org/10.5194/amt-12-6737-2019, 2019.
Xu, Z., Wang, T., Wu, J., Xue, L., Chan, J., Zha, Q., Zhou, S., Louie, P. K., and Luk, C. W.: Nitrous acid (HONO) in a polluted subtropical atmosphere: Seasonal variability, direct vehicle emissions and heterogeneous production at ground surface, Atmospheric environment, 106, 100-109, https://doi.org/10.1016/j.atmosenv.2015.01.061, 2015.
Ye, C., Gao, H., Zhang, N., and Zhou, X.: Photolysis of nitric acid and nitrate on natural and artificial surfaces, Environmental Science & Technology, 50, 3530-3536, https://doi.org/10.1021/acs.est.5b05032, 2016.
Ye, C., Zhang, N., Gao, H., and Zhou, X.: Photolysis of Particulate Nitrate as a Source of HONO and NO x, Environmental Science & Technology, 51, 6849-6856, https://doi.org/10.1021/acs.est.7b00387, 2017.
Yuan, H., Dai, Y., Xiao, Z., Ji, D., and Shangguan, W.: Reprocessing the MODIS Leaf Area Index products for land surface and climate modelling, Remote Sensing of Environment, 115, 1171-1187, https://doi.org/10.1016/j.rse.2011.01.001, 2011.
Zhang, J., An, J., Qu, Y., Liu, X., and Chen, Y.: Impacts of potential HONO sources on the concentrations of oxidants and secondary organic aerosols in the Beijing-Tianjin-Hebei region of China, Science of The Total Environment, 647, 836-852, https://doi.org/10.1016/j.scitotenv.2018.08.030, 2019.
Zhang, J., Lian, C., Wang, W., Ge, M., Guo, Y., Ran, H., Zhang, Y., Zheng, F., Fan, X., Yan, C., Daellenbach, K. R., Liu, Y., Kulmala, M., and An, J.: Amplified role of potential HONO sources in O_3 formation in North China Plain during autumn haze aggravating processes, Atmos. Chem. Phys., 22, 3275–3302, https://doi.org/10.5194/acp-22-3275-2022, 2022.
Zhang, L., Wang, T., Zhang, Q., Zheng, J., Xu, Z., and Lv, M.: Potential sources of nitrous acid (HONO) and their impacts on ozone: A WRF-Chem study in a polluted subtropical region, Journal of Geophysical Research: Atmospheres, 121, 3645-3662, https://doi.org/10.1002/2015JD024468, 2016.
Zhang, R., Sarwar, G., Fung, J. C., Lau, A. K., and Zhang, Y.: Examining the impact of nitrous acid chemistry on ozone and PM over the Pearl River Delta Region, Advances in Meteorology, 2012, https://doi.org/10.1155/2012/140932, 2012.

926 Zhang, Y., Shao, M., Lin, Y., Luan, S., Mao, N., Chen, W., and Wang, M.: Emission inventory of carbonaceous
927 pollutants from biomass burning in the Pearl River Delta Region, China, Atmospheric Environment, 76, 189-
928 199, https://doi.org/10.1016/j.atmosenv.2012.05.055, 2013.
929 Zhou, X., Zhang, N., TerAvest, M., Tang, D., Hou, J., Bertman, S., Alaghmand, M., Shepson, P. B., Carroll, M.
930 A., and Griffith, S.: Nitric acid photolysis on forest canopy surface as a source for tropospheric nitrous acid,
931 Nature Geoscience, 4, 440-443, https://doi.org/10.1038/ngeo1164, 2011.

932